Die Pharmazie

Pharmazie **2026**; 81(8): 52565
https://doi.org/10.31083/Pharmazie52565

Research Article

Molecular Docking and Prediction of ADMET/Drug-Likeness Properties of Potential Bioactive Anti-Rheumatoid Arthritis Compounds Isolated From the Essential Oil of *Capparis Spinosa* L. Leaves

Sahar AlMotwaa[1,*,†], Waad Al-Otaibi[2,†]

[1]Applied College, Shaqra University, 11961 Shaqra, Saudi Arabia
[2]Department of Chemistry, College of Science and Humanities, Shaqra University, 11961 Shaqra, Saudi Arabia
*Correspondence: saharm@su.edu.sa (Sahar AlMotwaa)
[†]These authors contributed equally.
Academic Editor: Hirofumi Takeuchi
Submitted: 3 April 2026 Revised: 9 July 2026 Accepted: 17 July 2026 Published: 25 August 2026

Abstract

Background: Rheumatoid arthritis (RA) is a chronic autoimmune disease and one of the most prevalent complex inflammatory disorders. *Capparis spinosa* L. (*C. spinosa*) is recognized for its diverse medicinal properties. Traditionally, the plant has been employed to alleviateconditions such as paralysis, gastrointestinal infections, rheumatism, diabetes, anemia, pain, and eye infections. This study aimed to investigate the potential interactions and predicted pharmacological relevance of major compounds identified in the essential oil of *C. spinosa* leaves using computational approaches. **Methods:** Drug-likeness potential was determined using Absorption, Distribution, Metabolism, Excretion, and Toxicity (ADMET) profiling and molecular docking. Gas chromatography–tandem mass spectrometry (GC–MS) was used to characterize the chemical composition of the essential oil. Drug-likeness studies were performed with SwissADME, while molecular docking was conducted using PyRx and BIOVIA Discovery Studio. **Results:** Fourteen major compounds were computationally screened against RA-associated molecular targets to evaluate their potential ligand–target interactions and drug-likeness characteristics. Absorption, Distribution, Metabolism, and Excretion (ADME) and drug-likeness were evaluated according to Lipinski's "rule of five" to determine whether the compounds exhibited suitable pharmacokinetic properties, consistent with criteria for pharmaceutical development. Six major phytoconstituents, i.e., tau-cadinol (M1), diisobutyl phthalate (M5), (Z)-3-hexenyl benzoate (M7), farnesyl acetone (M8), dibutyl phthalate (M10), and 1-(4-tert-butylphenyl)propan-2-one (M12), identified *via* GC–MS were docked with tumor necrosis factor-α (TNF-α), interleukin-6 (IL-6), interleukin-1β (IL-1β), nitric oxide synthase (NOS), and cyclooxygenase-2 (COX-2). This is the first report describing an *in silico* screening of GC–MS-identified compounds from *C. spinosa* for their predicted pharmacological potential. Docking ligand scores for all ligands against the target proteins ranged from –4.7 to –8.0 kcal mol^{-1}. Diisobutyl phthalate (M5) showed the most favorable binding energies against IL-1β and NOS, relative to the other compounds and co-crystallized ligands; meanwhile, tau-cadinol (M1) exhibited the highest binding energy for TNF-α. Six prevalent phytochemicals demonstrated highly favorable predicted docking affinities toward IL-6 and COX-2, with M10 showing the lowest docking energy values among the tested compounds under the applied computational conditions. **Conclusions:** These findings suggest that the examined phytochemicals may exhibit potential affinity toward RA-related molecular targets. As this is a preliminary computational investigation, the results should be interpreted with caution and warrant further computational and experimental studies to confirm their biological and therapeutic relevance.

Keywords: rheumatoid arthritis; *Capparis spinosa* L.; tumor necrosis factor-α; interleukin-6; interleukin-1β; nitric oxide synthase; cyclooxygenase-2; gas chromatography-mass spectrometry; molecular docking simulation

1. Introduction

Rheumatoid arthritis (RA) is a chronic autoimmune disease and one of the most common complicated inflammatory disorders [1]. While RA is incurable, early treatment may mitigate the risk of joint destruction and the associated distress while decelerating its development. The precise etiology of RA remains ambiguous, although evidence suggests that genetic and environmental conditions are involved [1]. The global prevalence of RA is approximately 1%, and it is more common in females than males, with a male to female ratio of 1:3 [2,3]. The management for RA is based on the use of disease-modifying anti-rheumatic drugs (DMARDs), glucocorticoids (GCs), and non-steroidal anti-inflammatory medications (NSAIDs). However, long-term administration of approved RA medications is correlated with deleterious adverse consequences. Moreover, some patients exhibit inadequate responses after using DMARDs [4]. There are several potential RA therapeutic targets for alleviating inflammation and oxidative stress in patients [5]. Cytokines have been extensively investigated as possible targets for RA drugs due to their direct involvement in the disease. Depending on their distinct roles in disease

response, cytokines are categorized into pro-inflammatory and anti-inflammatory classes. Studies have established that pro-inflammatory cytokines such as interleukin (IL)-1β, IL-6, and tumor necrosis factor-α (TNF-α) promote inflammation [4]. The levels of these pro-inflammatory cytokines have been found to be higher in the synovium, serum, and synovial fluid samples from RA patients than in healthy individuals. Moreover, these cytokines mediate the activation of T-cells, followed by chronic inflammation and tissue damage. Most anti-RA inhibitors are targeted at the reduction of levels of pro-inflammatory cytokines to reduce the RA symptoms and relieve pain [4].

Another potential strategy involves targeting nitric oxide synthase (NOS), thereby effectively managing RA-linked inflammation and its associated consequences. Elevated concentrations of nitric oxide (NO) in the plasma and joint fluid in patients with RA also cause health issues such as cardiovascular and neurological problems [6]. An increase in the activity of NOS leads to excessive production of NO. The raised level of NO aggravates RA by generating and releasing inflammatory cytokines, promoting angiogenic activity, raising vasodilation and permeability, and reacting with ROS to produce free radicals that cause oxidative stress [6]. Cyclooxygenase (COX) is considered a potential therapeutic target since NSAID therapeutic drugs like Naprelan, Mobic, and Duexis inhibit the activity of COX. Thus, COX inhibitor drugs are used for pain relief in RA patients. However, prolonged use of NSAIDs leads to severe complications such as hepatic and renal dysfunction [4].

Natural bioactive compounds have been extensively explored as potential scaffolds for novel anti-inflammatory drugs that inhibit the release of inflammatory mediators, given the undesirable side effects associated with NSAIDs [7,8]. Natural products represent a promising source of anti-inflammatory agents, owing to their extensive structural diversity. Furthermore, the utilization of medicinal plants in traditional medicine indicates their potential to serve as templates for the synthesis of natural resource-derived anti-inflammatory agents [7,9].

Capparis spinosa L. (*C. spinosa*) is a popular medicinal plant used in conventional medical treatments. The plant (*C. spinosa*), which is known locally in Saudi Arabia as Shaflah, belongs to the *Capparaceae* family. This plant is used widely in traditional medicine for the alleviation of a variety of diseases [10]. These diseases comprise paralysis, gastrointestinal infections, rheumatism, diabetes, stomachache, anemia, pain, eye infections, and kidney stones [10]. The biological activity of *C. spinosa* has earned considerable attention in both *in vivo* and *in vitro* investigations. Researchers have identified several pharmacological effects of *C. spinosa*, such as antiarthritic, antioxidant, diabetes-prevention, antitumor, liver protective, anti-inflammatory, neuroprotective, and antibacterial properties [11]. The major phytochemical compounds identified in the *C. spinosa* plant are flavonoids, alkaloids, volatile oils, fatty acids, and polysaccharides [11]. Recently, Sun et al. [11] suggested that, despite the identification of many different compounds in *C. spinosa*, additional research is required to fully unravel their biological effects and the associated mechanisms of action.

Computing and biomedical informatics are crucial to emerging drug discovery and evaluation [12]. Molecular docking enables assessment of binding strengths and drug-protein interactions, which are essential for drug development [13]. Moreover, investigations into the ADMET profiles are crucial for understanding the *in vivo* processing of a therapeutic compound, apart from providing important insights into the safety and efficacy profile of a drug [14]. The present study was aimed at determination of the chemical composition of the essential oil from the leaves of *C. spinosa* using gas chromatography- tandem mass spectrometry (GC-MS). The research was also aimed at conducting *in silico* ADMET studies to assess the pharmacokinetic and drug-like characteristics of the high-yield components of the essential oil. Moreover, *in silico* molecular docking will be used to evaluate the binding affinity of the six compounds with the most favorable ADMET properties against TNF-α, IL-1, IL-6, NOS, and COX proteins, which are crucial targets in RA pathways. Overall, the investigators attempted to explore the potential molecular affinities and predicted therapeutic relevance of compounds identified in the essential oil of *C. spinosa* leaves in relation to RA-associated targets.

2. Materials and Methods

Except as stated differently, all of the materials used in this investigation were purchased from Sigma (Johannesburg, Gauteng, ZA) and were of American Chemical Society (ACS) quality. Filter sheets, flexible measuring containers, Pyrex® glass equipment, sealed vials, and other laboratory supplies were purchased from Alrowad Company for Medical Instrument and Equipment Suppliers in Jeddah, SA. The highly sensitive digital balance, Clevenger instrument, and mechanical micropipettes of diverse measurements were procured from ALSAGGAF Scientific Solution Co. (Jeddah, SA). Alzamil Manufacturing, Commerce, and Logistics of Riyadh, SA, provided the water purification equipment.

2.1 Plant Material Collection and Preparation

The leaves of *Capparis spinosa* L. were harvested from wild specimens of the plant in the Riyadh region coordinates 25°19'00.8"N; 46°09'39.9"E, and stored in sealed plastic bags. The samples were dark-drying each separately for ten consecutive days at ambient temperature (25 ± 2 °C). The plant was collected by Essam Al-Sahli Trading Est.(Riyadh, SA) The plant was taxonomically identified and authenticated by Dr. Mona Alrasheed, Department of Biology, College of Science and Humanities, Shaqra Uni-

versity, Saudi Arabia. At the time of collection, no herbarium voucher specimen was deposited.

2.2 Isolation and Identification of C. spinosa Essential Oils

The essential oils of *C. spinosa* were produced using the hydro-distillation process of 0.2 kg of isolated, dark-drying leaves in 1.3 L of purified water at 60 °C for 3 h, utilizing Clevenger-type equipment (Pragati Scientific, Haryana, India).

2.3 Separation of Essential Oils and Assessment of Yield

The distilled aqueous phase of the extract comprising essential oil and leaf-extracted water was passed through filtered paper in a separatory funnel. Five milliliters of n-hexane were introduced into the separatory funnel for the extraction of the essential oil. The solvent partitioning procedure was conducted repeatedly to guarantee the total recovery of oil from aqueous solution. The n-hexane solvent was removed over the oil solution by rotational evaporation, and any remaining water was absorbed by anhydrous sodium sulfate. Prior to use in the study, the of *C. spinosa* essential oil was stored at 4 °C in a closed, light resistance bottle.

The percentage yield (Y) of *C. spinosa* essential oil was determined according to the subsequent equation:

$$Y = (Wo \times 100)/Mp$$

Wo is the amount of essential oil obtained, and Mp denotes the quantity of *C. spinosa* utilized in the isolation procedure.

2.4 GC-MS Identification for Chemical Constituents

The chemical composition of the *C. spinosa* leaves' essential oil was analyzed employing a Hewlett-Packard GC-MS system coupled to an Agilent 7000D triple quadrupole mass spectrometer (Agilent Technologies, Palo Alto, CA, USA). The HP-5MS column (30 m × 0.25 mm × 0.25 µm film thickness) was used to separate the samples, with helium serving as the carrier gas and a flow rate of 0.5 mL min^{-1}. An injected volume of 0.2 µL (1:10 n-hexane v/v) was used to conduct the analysis in split mode (1:25). The injector temperature was established at 250 °C, while the oven temperature was designed to increase from 60 °C (for 8 min) to 280 °C at a rate of 2 °C min^{-1}, subsequently held for 15 minutes. Mass spectra were acquired using electron impact (EI) ionization at 70 eV across a scan *m/z* range of 30–550. Constituents have been determined via the Automated Mass Spectral Deconvolution and Identification System (AMDIS) software (NIST, Gaithersburg, MD, USA) and by comparing their mass spectra against the Wiley and National Institute of Standards and Technology (NIST) mass spectral databases. For the identification of compounds, retention indices (RI) were computed in relation to an n-alkane calibration mixture (C8–C22) and utilized alongside retention times and mass spectral comparison. From the total of peak areas, relative percentages were ascertained. Plant sampling, essential oil extraction, and GC-MS determination were conducted singularly with one sample, without multiple replicates.

2.5 Chemical Identification of the Constituents of C. spinosa Essential Oil

The compounds were identified based on their structural classifications provided in the PubChem Library [15], with supplementary sources to the Kyoto Encyclopedia of Genes and Genomes (KEGG) -derived information in combination with the standardized Medical Subject Headings (MeSH) hierarchical vocabulary, where necessary. Each identified constituent received the associated PubChem Compound Identifier (CID) together with its GC-MS retention profile of the sample, which was based on its time of elution. Subsequently, compounds with proportions that are 0.5% or higher were chosen as screening ligands for further computational investigations. This threshold was applied to prioritize the major constituents with relatively higher abundance and a greater likelihood of contributing to the overall biological and pharmacological profile of the essential oil. In addition, the selected compounds were further evaluated based on structural diversity and preliminary drug-likeness and ADMET screening criteria.

2.6 In Silico Analysis

2.6.1 ADMET Profiling

It is crucial to determine the ADMET profiles of extracted compounds in the initial phase. The ADMET Predictor employs a structure-based computational platform designed to estimate the pharmacokinetic characteristics of drug-like compounds [16]. To be deemed a strong candidate, a medication or drug-like molecule must have other properties with respect to its high bioactivity and inadequate toxicity. Pharmacokinetic characteristics are a critical feature to consider when developing a novel drug. Simplified Molecular Input Line Entry System (SMILES) representations of the identified compound were generated in *sdf format and then converted into SMILES format using the NCI Chemical Identifier Resolver (CACTUS) (http://cactus.nci.nih.gov/translate/). The ADMET prediction was conducted using the pkCSM tool available online (https://biosig.lab.uq.edu.au/pkcsm/prediction) to assess pharmacokinetic properties such as absorption, distribution, metabolism, excretion, and toxicity [17,18]. The ADME characteristics of the chemical compound were predicted utilizing SwissADME, an online platform for ADME prediction (http://www.swissadme.ch) [19].

2.6.2 Computational Physicochemical Characterization

The predicted physicochemical descriptors comprised molecular mass, lipophilicity (LogP), molecular flexibility (rotatable bonds), topological polar surface area (TPSA), and hydrogen-binding capacity (donors and acceptors counts). These attributes demonstrate the bioavailability of drugs in the body, as delineated by Lipinski's rule of five [20]. Lipinski's Rule of Five is the most recognized rule-based criterion for evaluating its potential to exhibit favorable oral bioavailability. The criteria for the rule are as follows: the molecular mass of the compound must be ≤500, the hydrogen bond donor count should be ≤5, the hydrogen bond acceptor count should be ≤10, the optimal lipophilicity range measured in LogP should be ≤5, and the molar refractivity range should be 40–130. Consequently, a compound is not likely to be orally bioavailable as a drug if its properties deviate from these requirements [21].

2.7 Generation and Retrieval of Molecular Structures for Docking

To determine the potential repressive effects of the ligands on the targeted proteins, they were downloaded in two-dimensional (2D) *sdf format from PubChem (https://pubchem.ncbi.nlm.nih.gov/) [22]. Using the Online SMILES Translator (https://cactus.nci.nih.gov/translate/), the ligands were transformed into three-dimensional (3D) components in .pdb format for a facilitated and effective virtual screening process.

2.8 Structural Refinement of Target Receptors and Binding Pocket Determination

The crystalline configurations of TNF-α, IL-6, IL-1β, NOS, and COX-2 were retrieved in Protein Data Bank (PDB) files from the Research Collaboratory for Structural Bioinformatics PDB (RCSB PDB) (https://www.rcsb.org) [23]. These proteins were selected as therapeutic targets for RA. The preparation of the proteins was conducted employing Biovia Discovery Studio (2019) (Dassault Systèmes, Vélizy-Villacoublay, France). This process involved the removal of co-crystallized ligands, water molecules, and heteroatoms, along with the addition of hydrogen atoms to enhance the stability of the protein structure [24]. The active sites where ligands bind to induce conformational changes and trigger pharmacological responses were identified, thereby guiding docking simulations. The use of virtual screening to anticipate binding in these active sites not only decreases the expenses involved but also reduces the duration of drug discovery while enhancing binding precision [25]. The analysis of binding pockets and identification of ligand interactions and amino acid residues in the active sites were carried out using Biovia Discovery Studio [24].

2.9 Molecular Docking and Visualization

The docking procedure was conducted via PyRx software V0.8 with the Vina Wizard tool (https://pyrx.sourceforge.io/downloads/) to assess interactions between macromolecules and ligands [26]. Protein structures in PDB format were transformed into Protein Data Bank, Partial Charge (Q) and Atom Type (T) (PDBQT) employing the "make macromolecule" option. Each ligand was energy-minimized to optimize geometry, eliminate unfavorable torsions, and assure structural stability prior to conversion to PDBQT [26,27]. Each ligand and target molecule was prepared in a comparable manner. The ligands were considered flexible, while the receptor was maintained in a rigid conformation throughout the docking computations. Physiological pH-appropriate protonation states were assigned to ligand motifs and protein residues, and polarized hydrogen atoms were included. Docking was directed at experimentally determined active sites to accurately predict interactions. The amino acid residues in the active sites for ligands were determined using Biovia Discovery Studio. The COX-2 active site residues were determined according to Beura and Chetti [28]. Docking was performed at these coordinates using a grid box encompassing the active site in order to ensure precise modeling, as detailed in Table 1. The docking grid box was centered on the coordinates of the co-crystallized ligand to guarantee the inclusion of all essential active-site residues. The docking settings were configured with an exhaustiveness value of eight. The quantity of binding forms that were formed for each ligand was determined to be nine. The optimal binding position was chosen by considering minimal interaction free energy and advantageous interaction patterns. To validate this procedure, redocking the co-crystallized ligand compounds was accomplished for the different targets' active sites, thereafter calculating the root-mean-square deviation (RMSD) corresponding to the docked and experimental positions. Scores of RMSD less than 3 Å were deemed suggestive of satisfactory docking precision. Docking-related outcomes were depicted with Biovia Discovery Studio 2019 [24]. The complex exhibiting the lowest binding energy was utilized for analysis of type of interaction, length, and residues involved. Docking scores were determined by AutoDock Vina in PyRx software V0.8 (https://pyrx.sourceforge.io/downloads/) and expressed as kcal mol^{-1}, and the minimal binding energy was chosen for a comprehensive evaluation of protein-ligand interactions, encompassing interaction types, interaction lengths, and critical binding site residues.

3. Results

3.1 Chemical Composition of Essential Oil of C. spinosa Leaves

The hydro-distillation method for *C. spinosa* leaves using a Clevenger apparatus produced an essential oil yield of 0.2%. Analysis of the essential oil using gas chromatography (Fig. 1A) revealed the presence of 132 compounds,

Table 1. Docking grid coordinates and dimensions of selected proteins.

Proteins	Ligand ID	PDB	Grid box (x, y, z)	
			Center	Size
Interleukin-1 beta	JGY $C_{10}H_{15}N_3O_2$	5R8Q	37.1931022891	25.0
			0.488215278616	25.0
			72.2784260602	25.0
Inducible nitric oxide synthase	H2B $C_9H_{13}N_5O_3$	4NOS AC3	0.487377720998	25.0
			94.7466992304	25.0
			18.3466868452	25.0
Tumor necrosis factor-α (TNF-α)	307 $C_{32}H_{32}F_3N_3O_2$	2AZ5	–17.0573412297	20.0216140682
			70.6758175518	20.0145541745
			41.3928141841	20.0685874884
Interleukin-6	TLA $C_4H_6O_6$	1ALU AC5	–6.92863469578	25.0
			–9.75101525806	25.0
			–0.514955580666	25.0
Cyclooxygenase-2	COH $C_{34}H_{32}CoN_4O_4$ SAL $C_7H_6O_3$	5F1A	30.8542001557	25.0
			34.2608340072	25.0
			238.898317634	25.0

PDB, Protein Data Bank.

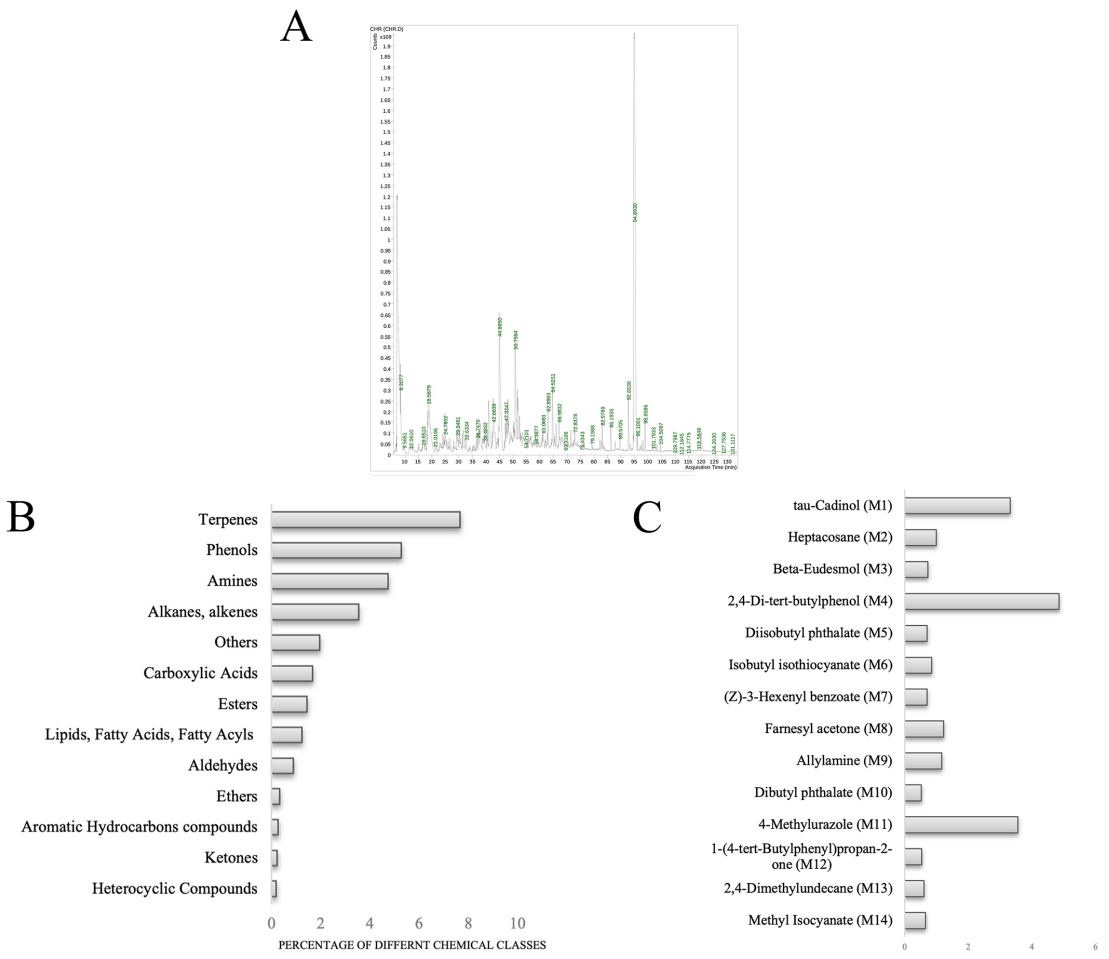

Fig. 1. GC-MS analysis. (A) Chromatogram of essential oil from *C. spinosa* leaves. (B) Major phytochemical composition of *C. spinosa*. (C) Major phytochemical constituents of *C. spinosa*. GC-MS, gas chromatography- tandem mass spectrometry.

Table 2. Assessments of drug-like properties of selected compounds (M1–M14) with the SwissADME platform.

	MW (g/mol)	#HA	#HD	MLOGP	LogP (iLOGP)	LogS	Lipinski #violations	TPSA (Å^2)	#RB	Veber #violations	Synthetic accessibility	MR
Rule	≤500	≤10	≤5	≤4.15	≤ 5		≤1	≤140	≤10	(Yes/No)	Easy (0)–difficult (10)	40 ≤ MR ≤ 130
M1	222.37	1	1	3.67	3.14	–3.26	0	20.23	1	0	4.29	70.72
M2	380.73	0	0	8.86	7.32	–9.59	1	0	24	1	3.56	131.9
M3	222.37	1	1	3.67	3.06	–3.51	0	20.23	1	0	3.38	70.46
M4	206.32	1	1	3.67	3.06	–4.55	0	20.23	2	0	1.43	67
M5	278.34	4	0	3.43	3.31	–3.85	0	52.60	8	0	2.36	77.84
M6	115.20	1	0	2.48	2.27	–2.20	0	44.45	2	0	1.83	35.31
M7	204.26	2	0	3.31	3.04	–3.55	0	26.30	6	0	2.14	61.28
M8	262.43	1	0	4.50	4.08	–4.38	1	17.07	9	0	3.47	87.42
M9	57.09	1	1	0.15	1.28	–0.15	0	26.02	1	0	1.01	18.77
M10	278.34	4	0	3.43	2.97	–3.96	0	52.60	10	0	2.41	77.84
M11	115.09	2	2	–0.82	0.46	–0.47	0	70.65	0	0	1.30	26.94
M12	190.28	1	0	3.25	2.50	–3.16	0	17.07	3	0	1.26	60.49
M13	184.36	0	0	5.67	3.77	–4.66	1	0	8	0	2.39	64.60
M14	57.05	2	0	–0.59	1.29	–0.86	0	29.43	0	0	1.23	13.99

MW, molecular weight; #HA, H bound acceptor count; #HD, H bound donor count; MR, Molar Refractivity; LogP (iLOGP), octanol/water partition coefficients; TPSA, Topological polar surface area; MLOGP, Moriguchi LogP (lipophilicity parameter); LogS, log of the aqueous solubility; #RB, number of rotatable bonds, #; Number of.

Table 3. *In silico* ADMET profiling for the selected compounds (M1–M14) obtained from SwissADME and pkCSM.

	Absorption				Distribution		Metabolism							
							Substrate			Inhibitor				
							CYP							
	Skin permeability	P-gp substrate	GI	VDss (human)	BBB permeability	CNS permeability	2D6	3A4	1A2	2C19	2C9	2D6	3A4	1A2
	Log Kp (cm/s)	Categorical (Yes/No)	Categorical (High/Low)	Log L/kg	Categorical (Yes/No)	Log PS	Categorical (Yes/No)							
M1	–5.29	No	High	0.415	Yes	–2.032	No	Yes	No	Yes	No	No	No	No
M2	1.49	Yes	Low	0.247	No	–0.817	No	Yes	Yes	No	No	No	No	No
M3	–5.00	No	High	0.442	Yes	–1.828	No	Yes	Yes	No	Yes	No	No	No
M4	–3.87	No	High	1.018	Yes	–1.236	No	Yes	Yes	No	No	Yes	No	No
M5	–5.08	No	High	–0.139	Yes	–2.192	No	Yes	Yes	Yes	No	No	No	Yes
M6	–5.00	No	High	0.028	Yes	–2.181	No	No	No	No	No	No	No	No
M7	–4.68	No	High	0.196	Yes	–1.719	No	No	Yes	Yes	No	No	No	Yes
M8	–3.95	No	High	0.438	No	–1.720	No	Yes	Yes	No	Yes	No	No	Yes
M9	–6.63	No	High	0.284	No	–2.518	No	No	No	No	No	No	No	No
M10	–4.80	No	High	–0.007	Yes	–2.408	No	Yes	Yes	Yes	No	No	No	Yes
M11	–7.62	No	High	–0.462	No	–3.482	No	No	No	No	No	No	No	No
M12	–5.18	No	High	0.541	Yes	–1.462	No	Yes	Yes	No	No	Yes	No	No
M13	–2.68	No	Low	0.559	No	–1.474	No	No	No	No	Yes	No	No	No
M14	–5.90	No	High	–0.229	No	–2.500	No	No	No	No	No	No	No	No

Abbreviations: BBB, blood-brain barrier, CYP, cytochromeP450, GIA, gastrointestinal absorption; LogKp, skin permeation value; P-gp, P-glycoprotein; GI, gastrointestinal; VDss, volume of distribution at steady state; CNS, central nervous system; Log L/kg, log of the volume of distribution at steady state; Log PS, log of the permeability surface-area product for CNS. Data of BBB and GIA according to the yellow/white yolk of a boiled egg chart respectively.

Table 4. Computational for excretion and toxicological for the selected compounds (M1–M14) predicted by ProTox-II.

Ligand no.	Total clearance (log mL/min/kg)	Renal OCT2 substrate	Skin sensitization	Toxicity								
				Immuno	Hepato	Cyto	Carcino	Mutagen	Nephro	AMES	LD_{50} (mg/kg)	Toxicity class
M1	1.085	No	Yes	Yes	No	No	No	No	No	No	2830	5
M2	2.093	No	Yes	No	No	No	No	No	No	No	750	3
M3	1.032	No	Yes	No	No	No	No	No	No	No	2000	4
M4	0.912	No	Yes	No	No	No	No	No	No	No	700	4
M5	0.800	No	No	No	No	No	Yes	No	Yes	No	10,000	6
M6	0.426	No	Yes	No	No	No	No	No	No	No	112	3
M7	0.867	No	Yes	No	No	No	Yes	No	No	No	5000	5
M8	1.726	No	Yes	No	No	No	No	No	No	No	5000	5
M9	0.999	No	No	No	No	No	Yes	No	No	No	57	3
M10	0.930	No	No	No	No	No	Yes	No	Yes	No	3474	5
M11	0.996	No	No	No	Yes	No	No	No	Yes	No	134	3
M12	0.249	No	Yes	No	No	No	Yes	No	No	No	3500	5
M13	1.497	No	Yes	No	No	No	No	No	No	No	750	3
M14	0.808	No	No	No	No	No	Yes	No	No	No	52	3

OCT2, organic cation transporter 2; AMES, AMES mutagenicity test; LD_{50}, Oral Rat Acute Toxicity (median lethal dose).

as detailed in **Supplementary Table 1**. The identities of the compounds were determined by comparing their mass spectra with NIST reference data. Compounds with similarity scores exceeding 80 were considered reliably identified. The selected compounds constituted 30% of the total components. The compounds comprised terpenes (7.66%), phenols (5.27%), amines (4.73%), alkanes and alkenes (3.55%), lipids, fatty acids, and fatty acyls (1.22%); carboxylic acids (1.66%), esters (1.44%), aldehydes (0.88%), ethers (0.33%), aromatic hydrocarbon compounds (0.27%), ketones (0.21%), heterocyclic compounds (0.17%), and others such as sulfur, isocyanates, and halogen compounds (1.94%). These results are shown in Fig. 1B. To facilitate computational screening against RA-associated molecular targets, fourteen compounds with relative abundances exceeding 0.5% were selected, as listed in Fig. 1C.

3.2 ADME Analysis and Toxicity Prediction

The ADMET features of the essential oil of *C. spinosa* leaves were assessed using *in silico* approaches to ascertain its potential as a drug candidate. The potential drug-likeness of a chemical compound isolated in high yield is assessed through Lipinski's "rule of five". Lipinski's rule delineates that the major compound possesses a molecular weight (MW) of 500 or less, a LogP value (octanol–water partition coefficient) of 5 or lower, a maximum of five hydrogen bond donors (HDO), and no more than ten hydrogen bond acceptors (HAC) [29]. Based on the findings in Table 2, Lipinski's rule was obeyed by all selected phytochemicals. The MW of compound M2 (381 g/mol) satisfied Lipinski's rule. All the selected compounds exhibited proficient lipophilicity scores (LogP values ranging from 0.46 to 4.08), except for M2, which had a very high lipophilicity score (7.32). All the compounds (M1–M14) had acceptable HDO and HAC bonds. The solubility of a compound is typically represented as log of the aqueous solubility (LogS). Approximately 85% of pharmaceuticals exhibited LogS values ranging from –1 to –5, with virtually none falling below –6 [30]. Ten of the 14 selected compounds exhibited LogS values ranging from –1 to –5, indicating excellent-to-moderate water solubility. Compound M2 had poor solubility, while M9, M11, and M14 exhibited high solubility values. Notably, the highest solubility compounds, M9, M11, and M14 had the smallest MWs (115.2, 57.05, and 57.09, respectively) and molar refractivity (MR) less than 30.

The Veber rule indicates that compounds exhibiting a TPSA $\leq$140 Å^2 and/or number of rotatable bonds (RB) $\leq$10 provide favorable oral bioavailability [31]. In this study, all the compounds (M1–M14) adhered to Veber's rule, while one compound exhibits a single violation due to the increased number of RBs bound. The TPSA value ranged from 0 to 70.65 Å^2. Each compound under investigation had $\leq$10 RB, except for M2, which had 24 RB. Our finding indicates that 9 out of the 14 compounds were within the MR specified range. The highest recorded value of MR for M2 was more than 130. In contrast, M6, M9, M11, and M14 had MR values less than 40. The synthetic accessibility of the 14 compounds ranged from 1.01 to 4.29, indicating that they are readily synthesized. In addition, all 14 compounds achieved an excellent bioavailability score of 0.55.

Skin permeability is represented byLog Kp (cm/s) with a reference range of –8.0 to –1.0 [32]. The logKp values for all compounds in this investigation, except for M2, ranged from –2.68 cm/s to –7.62 cm/s, indicating effective transdermal permeability (Table 3). The P-glycoprotein (P-gp) transporter is a protein that significantly influences drug absorption [33]. This protein (P-gp) mediates the transfer of substrates into the bile, urine, and the gastrointestinal (GI) tract [34]. The ADMET results (Table 3) indicate that all the drug candidates, with the notable exception of M2, were not substrates for P-gp. GI absorption is a major factor that affects drug kinetics and the efficacy of compounds [35]. The results indicate that compounds M2 and M13 were associated with poor intestinal absorption, while the other compounds exhibited excellent intestinal absorption.

The ADMET prediction of volume of distribution at steady state (VDss) and blood-brain barrier (BBB) permeabilities were used to assess the distribution of the compounds under examination within the human body (Table 3). The VDss indicates the tendency of a drug to remain in the plasma or to diffuse into other tissue compartments. Log VDss <–0.15 implies poor distribution, whereas Log VDss >0.45 implies high distribution [36]. Table 3 shows VDss values of –0.462 L/kg and –0.229 L/kg for M11 and M14, respectively. The VDss values for M12 (0.541 L/kg) and M13 (0.559 L/kg) were slightly above the recommended range, while M4 had the highest VDss value of 1.018 L/kg. All the other compounds were within the recommended VDss range. The BBB acts as a selective filter by restricting the entry of substances into the central nervous system (CNS) [37]. The molecules M1, M3–M7, M10, and M12 exhibited BBB permeability, whereas the ligands M2, M8, M9, M11, M13, and M14 exhibited poor capacity to pass through the BBB.

The cytochrome P450 (CYP450) system is responsible for the metabolism and removal of drugs from the body. An understanding of how substances interact with CYP450 is crucial for characterizing the pharmacokinetics of potential drugs during drug development [19]. The potential inhibitors for two of CYP450 were M5, M7, M8, and M10, while M1, M3, M4, M12, and M13 tended to inhibit 1 isoform of CYP450. The compounds M2, M6, M9, M11, and M14 did not show an inhibitory effect on the CYP450 isoforms. It was predicted that M1–M5, M8 and M10 are potential substrates for CYP3A4, whereas all the compounds are not likely to be substrates for 2D6.

The excretion of pharmacological molecules may be predicted by assessing total clearance (log mL min^{-1} kg^{-1}) and their potential as substrates for renal organic cation

transporter 2 (OCT2) (Table 4). Clearance refers to the quantity of a chemical molecule eliminated from plasma in the vascular compartment per unit time [38]. The overall clearance score comprises all liver and kidney clearances of the chemicals eliminated through the kidneys [38,39]. Compound M2 had the highest overall clearance score, which signifies effective excretion from the body, whereas M6 and M12 presented the lowest outcomes, thereby indicating relatively slower clearance rates. Renal OCT2 is a renal uptake transporter that significantly contributes to renal clearance and the elimination of drugs and endogenous substances [40]. In this study, the predictions indicate that none of the 14 compounds is a likely substrate for OCT2. Thus, the compounds will not exert a negative impact on renal clearance.

Regarding skin sensitization, M5, M9, M10, and M11 showed no evidence of skin sensitization, whereas the other compounds were associated with skin sensitization (Table 4). A prediction of toxicity is crucial to guarantee the safety of drugs, thereby ensuring the absence of harm or adverse effects. Results from hepatotoxicity revealed a positive effect only with M11. Moreover, only M1 demonstrated positive immunotoxicity. All the compounds did not exert nephrotoxicity, except for M5, M10, and M11, while M5, M7, M9, M10, M12, and M14 showed potential for carcinogenicity. These predicted toxicological concerns may limit the translational potential of some compounds and highlight the need for further optimization and experimental safety validation before therapeutic application.

However, the predictions revealed that none of the compounds were cytotoxic or mutagenic. Ames toxicity serves as an indicator for assessing the mutagenicity potential of drugs [41]. None of the investigated compounds exhibited Ames toxicity.

LD_{50}, also known as the 50% lethality threshold, is utilized for predicting acute toxicity. It is classified into six toxicity classes defined by the following threshold values: fatal if swallowed: LD_{50} less than 5 mg/kg; fatal if swallowed: LD_{50} of 5 to 50 mg/kg; toxic if swallowed: LD_{50} of 50 to 300 mg/kg; harmful if swallowed: LD_{50} more than 300 to 2000 mg/kg; may be harmful if swallowed: LD_{50} more than 2000–5000 mg/kg; and non-toxic: LD_{50} more than 5000 mg/kg body weight [42]. Table 4 displays the toxicity predictions, with a class 6 prediction value for M5, while M1, M7, M8, M10, and M12 had class 5 predictive values. Toxicity level 4 was predicted for M3 and M4, while M2, M6, M9, M11, M13, and M14 were assigned a toxicity class of 3. The predictive outcomes identified 6 compounds in toxicity classes of 5 and 6. The toxicity classification led to the exclusion of all potentially toxic compounds. Although several compounds showed promising pharmacokinetic and docking profiles, the predicted toxicological concerns highlight the need for careful safety evaluation and further *in vitro* and *in vivo* validation.

3.3 Molecular Docking Studies

This study involved a molecular docking analysis aimed at examining the predicted interactions of major phytochemicals derived from the essential oil of *C. spinosa* with the proteins IL-1β, NOS, TNF-α, IL-6, and COX-2, as computationally relevant RA-associated targets.

The interactions in biological systems, particularly ligand-protein interactions, involve various physical forces such as hydrophobic electrostatic forces, hydrogen bonding, ionic bonding, and van der Waals (VDW) forces. A potential inhibitor typically possesses an adequate number of hydrogen bonds and additional hydrophobic interactions which are crucial for protein-ligand interactions [43]. The binding affinity of a ligand to a protein is a measure of its strength, which is expressed in kcal/mol. Stronger interactions are indicated by lower binding affinity values. This is because the fact that the system releases more energy upon binding, resulting in a more stable complex. However, in general, more negative binding affinity values represent stronger binding interactions. Binding affinity values below –5 kcal/mol are generally considered indicative of potentially favorable ligand–protein interactions in computational docking studies. Binding interactions are classified as moderate when values range from –5 to –3 kcal/mol, whereas those exceeding –3 kcal/mol are deemed weak interactions [44,45]. The RMSD is used to evaluate the effectiveness of predicted ligand binding pose [46]. An RMSD value of 3.0 Å or less is generally regarded as acceptable [47]. In the present study, the docked ligand scores for all ligands (i.e., M1, M5, M7, M8, M10, and M12) targeting the proteins IL-1β, NOS, TNF-α, IL-6, and COX-2 ranged from –4.7 to –8 kcal mol^{-1}. All RMSD values for target ligand-protein interactions that were equal to or greater than 3 Å were omitted from consideration (Table 5).

The molecular docking results for six selected compounds inside the active site of IL-1β protein (PDB: 5R8Q) are presented in Table 6 and Fig. 2. The predicted active site residues of the target protein were the amino acids TYR24, GLU25, LEU26, LEU69, LEU80, PRO131, and VAL132. The redocking of the co-crystallized ligand produced a docking score of –5.4 kcal/mol, with an RMSD of 1.802 Å. Three hydrogen bonds were implicated in the interaction of the ligand with IL-1β residues: one bond with each of VAL132, LEU80 and TYR24. The candidate compounds exhibited predicted binding energy scores between –4.7 and –5.6 kcal/mol. The compound M1 exhibited hydrophobic bond interactions with the PRO131 residue of the protein. The M5 compound, with a docking score of –5.6 kcal/mol, had two-carbon-covalent hydrogen bonds with LEU26, and VAL132, along with hydrophobic interactions involving one bond with VAL132 and two bonds with residue PRO131. Compound M7 formed a hydrogen bond with LEU80, whereas M8 exhibited the weakest interaction among the selected phytochemical compounds through an alkyl bond with PRO131. The compound M10 formed a

Table 5. Binding energy and RMSD outcomes for six selected ligands with targeted proteins (PDB: 5R8Q, 4NOS, 2AZ5, 1ALU, and 5F1A) and their corresponding co-crystallized ligand.

Ligands	E	Target proteins Binding energy (kcal mol^{-1}) (RMSD in Å)				
		5R8Q INTERLEUKIN-1 BETA	4NOS NITRIC OXIDE SYNTHASE	2AZ5 TNF-α	1ALU INTERLEUKIN-6	5F1A Cyclooxygenase-2
M1	290.69	–5.2 1.349 (Å)	–6.8 1.471(Å)	–6.7 2.352 (Å)	–4.8 2.080 (Å)	–7.3 2.015 (Å)
M5	200.16	–5.6 1.768 (Å)	–8.0 2.610 (Å)	–6.4 2.624 (Å)	–5.0 2.240 (Å)	–7.3 2.690 (Å)
M7	99.61	–4.7 2.038 (Å)	–7.8 2.966 (Å)	–6.0 1.393 (Å)	–4.7 0.601(Å)	–6.9 1.771(Å)
M8	221.96	–5.0 1.527 (Å)	–7.6 2.474 (Å)	–6.4 2.050 (Å)	–5.1 2.963 (Å)	–6.7 2.147 (Å)
M10	160.54	–5.2 2.415 (Å)	–7.5 2.564 (Å)	–6.3 2.042 (Å)	–5.6 0.483 (Å)	–7.5 0.433 (Å)
M12	117.68	–5.4 0.240 (Å)	–6.7 2.604 (Å)	–6.0 2.630 (Å)	–4.7 1.152 (Å)	–6.0 2.974 (Å)
Co-crystallized Ligand						
JGY	293.51	–5.4 1.802 (Å)	-	-	-	-
H2B	136.56	-	–7.1 1.513 (Å)	-	-	-
307	495.60	-	-	–7.4 1.584 (Å)	-	-
TLA	20.28	-	-	-	–4.0 2.398 (Å)	-
COH	1043.53	-	-	-	-	–10.5 1.614 (Å)
SAL	90.10	-	-	-	-	–5.8 1.966 (Å)

RMSD, root-mean-square deviation; PDB, Protein Data Bank.

carbon hydrogen bond with VAL132 and a hydrophobic interaction with LEU26, while M12 displayed a conventional hydrogen bond with LEU80 and LEU134.

The binding affinities of the selected ligands to the NOS protein (PDB: 4NOS), as well as 2D and 3D illustrations, are displayed in Table 7 and Fig. 3. The putative active site residues of the NOS protein were TRP194, ARG199, CYS200, GLN205, SER242, PHE369, ASN370, TRP372, GLU377, TRP463, TYR489, TYR490, and TYR491. All ligands under consideration exhibited potentially favorable binding interactions with the key residues in the active site, as indicated by their docking scores and binding conformations, except for M1. The binding energy scores were between –6.7 and –8 kcal/mol, with compound M5 having the best binding energy score of –8 kcal/mol. Compounds M5, M7, and M12 demonstrated conventional hydrogen bonds with TRP194, as well as a variety of hydrophobic interactions with TRP194, PHE369, CYS200, and TYR489. Compounds M5 and M12 formed two amide-pi stacks with ASN370, while compound M8 had conventional hydrogen bond interactions with ARG199, in addition to numerous hydrophobic interactions with TRP194 (6), CYS200 (2), HE369 (3), and TYR489. Compound M10 exhibited a conventional hydrogen bond with TYR489, alongside hydrophobic interactions involving ARG199, TRP194 (2), CYS200, and HE369. The co-crystallized ligand formed three hydrogen bond interactions: two conventional bonds with GLU377 and one carbon-hydrogen bond with ASN370, alongside hydrophobic interactions with TRP194 and PHE369.

As shown in Table 8 and Fig. 4, the active site residues of TNF-α (PDB: 2AZ5) were LEU57, SER60, TYR119, LEU120, GLY121, GLY122, and TYR151. Among the studied ligands, M1 had the highest binding energy of –6.7 kcal/mol, while M7 and M12 recorded the least value of −6.0 kcal/mol. For all the explored compounds, it was revealed that the interactions established were mainly hydrogen bonds and hydrophobic interactions. The ligand M1 engaged with the receptor through the establishment of a conventional hydrogen bond with SER60, alongside

Table 6. Docking outcomes of major selected compounds in the essential oil from *C. spinosa* leaves and co-crystallized ligand against IL-1β protein (PDB: 5R8Q).

Ligand	Hydrogen bonds (Distance Å)	Hydrophobic interaction (Distance Å)
JGY	Conventional Hydrogen Bond: BB HAC: O=C VAL132 to –NH (2.52) BB HAC: O=C LEU80 to -NH (2.27) Carbon Hydrogen Bond: BB HDO: O=C TYR24 to H-C (3.53)	-
M1	Conventional Hydrogen Bond: BB HAC: O=C LEU 134 to -HO (2.34) Carbon Hydrogen Bond: SC HDO: H-C- LYS77 to -OH (3.58)	Alkyl: LYS77, PRO131 (4.92, 3.58) π–Alkyl: PHE133, PHE133 (4.34, 4.732)
M5	Carbon Hydrogen Bond: BB HAC: O=C LEU26 to H-C (3.63) BB HAC: O=C VAL132 to H-C (3.41)	Alkyl: VAL132 (5.059) π–Alkyl: PRO131, PRO131 (5.08, 4.21)
M7	Conventional Hydrogen Bond: BB HDO: -NH LEU80 to O=C (1.78) BB HDO: -NH LEU134 to O=C (2.09) Carbon Hydrogen Bond: BB HAC: O=C LEU134 to H-C (3.59)	π–Alkyl: PHE133, PHE133 (4.80, 5.14)
M8	-	Alkyl: LYS77, PRO131 (4.79, 5.25)
M10	Carbon Hydrogen Bond: BB HAC: O=C VAL132 to H-C (3.73)	Alkyl: LEU26, LEU82 (4.89, 4.27) π–Alkyl: PHE 133 (3.99)
M12	Conventional Hydrogen Bond BB HDO: HN- LEU80 to (2.11) O=C BB HDO: HN- LEU134 to (2.16) O=C	π–Sigma: PHE 133 (3.84) π–π Stacked: PHE 133 (4.59) π–Alkyl: PHE 133 (4.49)

Active site (PDB: 5R8Q): TYR24, GLU25, LEU26, LEU69, LEU80, PRO131, VAL132. BB, Backbone atoms; SC, Side chain atoms; HDO: H bound donor, HAC, H bound acceptor.

two alkyl interactions with LEU57 and two π–alkyl interactions with TYR119 and TYR151. With respect to compounds M5 and M10, it was observed that conventional hydrogen bond interactions were formed with the residue GLY121, in combination with various hydrophobic interactions such as π–π stacking, π–sigma, π–alkyl, and amide-π stacked bonds, with TYR119. Compound M10 presents an additional π–alkyl interaction with TYR151. Compounds M7 and M12 established two conventional hydrogen bonds with residues GLY121 and TYR151, as well as hydrophobic interactions with TYR119 in the form of π–π stacked, π–sigma, and π–alkyl bonds. Compound M8 established a conventional hydrogen bond with residue TYR151, together with hydrophobic interactions with LEU57 as an alkyl and with TYR119 and TYR151 as π–alkyl. The co-crystallized ligand halogen formed a conventional hydrogen bond with TYR151, and the halogen (fluorine) bound with SER60 (3). Many hydrophobic interactions were observed with TYR119 as π–π–stacked; LEU57 and TYR119 (2) as π–sigma, along with TYR119 (2), TYR151, and LEU57 as π–alkyl. In this investigation, all six compounds exhibited interactions with amino acid residues similar to those of the co-crystallized ligand.

The analysis of the docking results for IL-6 (PDB: 1ALU), as presented in Table 9, revealed that TLA, a co-crystallized ligand, exhibited a binding energy of –4 kcal/mol, accompanied by one hydrogen bond interaction with ARG182. The binding affinities of the six prevalent phytochemicals present in the essential oil of *C. spinosa* ranged from –4.7 to –5.6 kcal/mol. The active site of IL-6 comprised the amino acids GLN175, LEU178, ARG179, and ARG182. The chemical bonding interactions in the complexes between the examined compounds and the binding pocket residues of IL-6 are illustrated in Fig. 5. Compound M8 exhibited binding at the active site of the protein, forming three conventional hydrogen bonds with the two amino acids ARG179 and ARG182, and it exhibited hydrophobic interactions with LEU178. Hydrophobic interactions favored the binding of M5 and M10 to the active site of IL-6, which specifically involved LEU178 (for both M5 and M10) and LEU179 (for M10 only). The compound M7 interacted through one conventional hydrogen bond with GLN175 and three alkyl interactions with the amino acids LEU178, LEU178, and ARG182. Analysis of the best docked poses for M12 indicated the presence of a conventional hydrogen bond with ARG179 and a hydrophobic π-sigma interaction with LEU178.

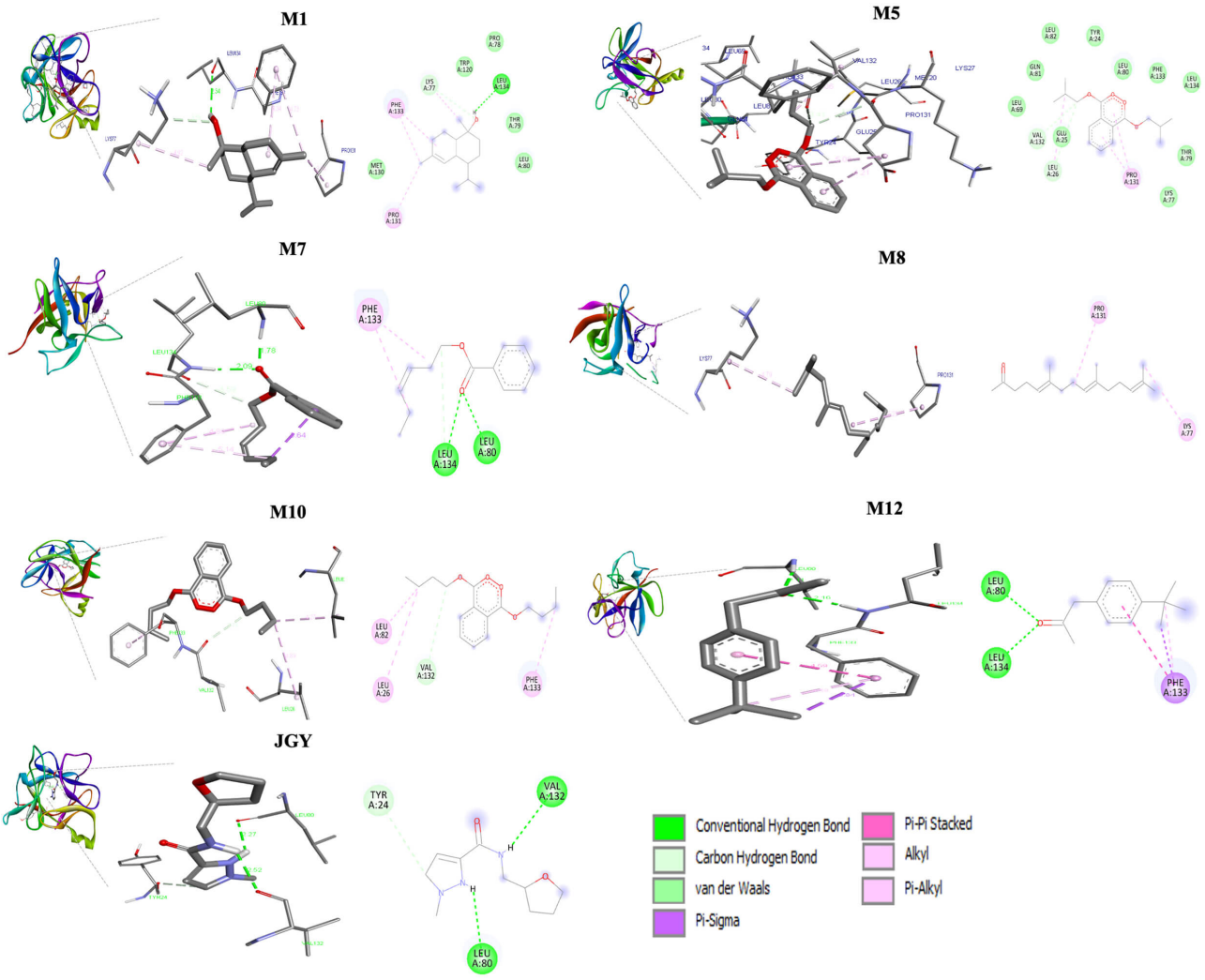

Fig. 2. 2D and 3D molecular interactions of the most prevalent selected compounds: M1, M5, M7, M8, M10, and M12 with the co-crystallized ligand "JGY" in the binding site of the IL-1β protein (PDB: 5R8Q).

All the explored compounds were docked into the active site of cyclooxygenase-2 (PDB: 5F1A). The interactions of the studied compounds in both 2D and 3D configurations are illustrated in Table 10 and Fig. 6. The examined compounds engaged with amino acid residues through conventional hydrogen bonds and hydrophobic interactions, with binding scores between −6.7 and –7.5 kcal/mol. The binding affinities of the six prevalent phytochemicals were greater than those of the co-crystallized ligand (SAL), with M10 possessing the highest affinity. In this context, compound M1 exhibited conventional hydrogen bonding interactions with HIS388, along with alkyl bonds with ALA202 and LEU391, as well as π–alkyl interactions with HIS207, HIS386, HIS386, HIS386, HIS386, and HIS388. Compound M5 demonstrated a hydrogen bonding interaction with HIS388. Furthermore, interactions of the π–π T-shaped, π–alkyl, and alkyl types occurred with HIS207, HIS386, LEU390, and LEU391, respectively. Compounds M7 and M10 exhibited two conventional hydrogen bonding interactions with TRP387 and HIS388, in addition to an alkyl interaction with LEU391 and a π−alkyl interaction with ALA202. Compound M10 formed extra π−alkyl interactions with PHE200, HIS207, HIS386, and LEU391 (2) residues, while M8 exhibited hydrophobic interactions with HIS386 through π−sigma binding ALA202 and LEU391 (2) via alkyl interactions and also with HIS207, TRP387, and PHE395 through π−alkyl binding. Compound M12 exhibited a conventional hydrogen bonding interaction with HIS388, in addition to π−alkyl and alkyl interactions with LEU391. When compared with the investigated ligand, the co-crystallized ligand SAL showed a hydrogen bonding interaction with HIS388. Additionally, there was an amide−π stacked interaction with TRP387 and π−alkyl bonds with ALA202 and LEU390. In contrast, the crystallized ligand displayed conventional hydrogen bonding interactions with HIS214 and THR212, alongside π–π T-shaped interactions with HIS207 and alkyl interactions with ALA202, LEU390, and LEU391 (2), as well

Table 7. Docking outcomes of major selected compounds in the essential oil from *C. spinosa* leaves and co-crystallized ligand against NOS protein (PDB: 4NOS).

Ligand	Hydrogen bonds (Distance Å)	Hydrophobic interaction (Distance Å)
H2B	Conventional Hydrogen Bond: BB HDO: HN-VAL352 to C=O (1.99) SC HAC: C-O GLU377 to -NH (2.63) SC HAC: C-O GLU377 to -NH (1.81) Carbon Hydrogen Bond: SC HDO: H-C- ASN370 to C=O (3.71)	π–Sigma: TRP194, TRP194 (3.72, 3.76) Alkyl: LEU209 (5.06) π–Alkyl: PHE369, PRO350 (4.95, 4.72)
M1	-	-
M5	Conventional Hydrogen Bond: SC HDO: H-C- TRP194 to O (2.73)	π–Sigma: TRP194, TRP194, PHE369 (3.76, 3.76, 3.85) Amide-Pi Stacked: ASN370, ASN370 (4.00, 4.61) Alkyl: MET374 (5.17) π–Alkyl: TRP194, TRP194, PHE369, CYS200, PRO350 (3.98, 4.55, 3.93, 4.91, 5.34)
M7	Conventional Hydrogen Bond: SC HDO: -NH TRP194 to C=O (2.88)	π–π–Stacked: TRP194, TRP194, PHE369 (3.62, 4.25, 4.21) Alkyl: A197, CYS200, CYS200, (3.62, 4.05, 4.62) π–Alkyl: PHE369, PHE369, TYR489, LEU209 (5.38, 4.72, 5.21, 5.44)
M8	Conventional Hydrogen Bond: BB HDO: -NH ARG199 to C=O (2.21)	π–Sigma: TRP194 (3.60) Alkyl: CYS200, VAL352, CYS200, LEU209 (4.35, 5.46, 4.65, 4.06) π–Alkyl: TRP194, TRP194, TRP194, TRP194, TRP194, PHE369, PHE369, PHE369, TYR489 (4.39, 3.95, 4.11, 4.78, 4.68, 5.36, 5.15, 4.05, 4.57)
M10	Conventional Hydrogen Bond: BB HAC: -C=O TYR489 to H-C- (3.65)	Alkyl: LEU209, ARG199 (4.41, 3.84) π–Alkyl: TRP194, TRP194, PHE369, ALA197, CYS200, CYS200 (3.90, 4.73, 5.11, 3.93, 4.46, 4.44)
M12	Conventional Hydrogen Bond: SC HDO: -NH TRP194 to O (2.73)	π–Sigma: TRP194, TRP194, PHE369 (3.76, 3.76, 3.85) Amide-Pi Stacked: ASN370, ASN370 (4.61, 4.00) Alkyl: MET374 (5.17) π–Alkyl: TRP194, TRP194, PHE369, CYS200, PRO350 (3.97, 4.55, 3.93, 4.91, 5)

Active site (PDB: 4NOS): TRP194, ARG199, CYS200, GLN205, SER242, PHE369, ASN370, TRP372, TRP372, GLU377, TRP463, TYR489, TYR490, TYR491. BB, Backbone atoms; SC, Side chain atoms; HDO, H bound donor; HAC, H bound acceptor; NOS, nitric oxide synthase.

as π−alkyl interactions with PHE200, TRP387, PHE395, LEU391, HIS207, PHE210, and HIS386. The active sites were identified according to the procedure of Satyajit Beura and Prabhakar Chetti [28]. Therefore, the examined phytochemicals have the potential to serve as targets for RA. To our knowledge, this represents the inaugural report in which bioactive compounds derived from *C. spinosa* have been subjected to molecular docking for the purpose of screening their pharmacological potential.

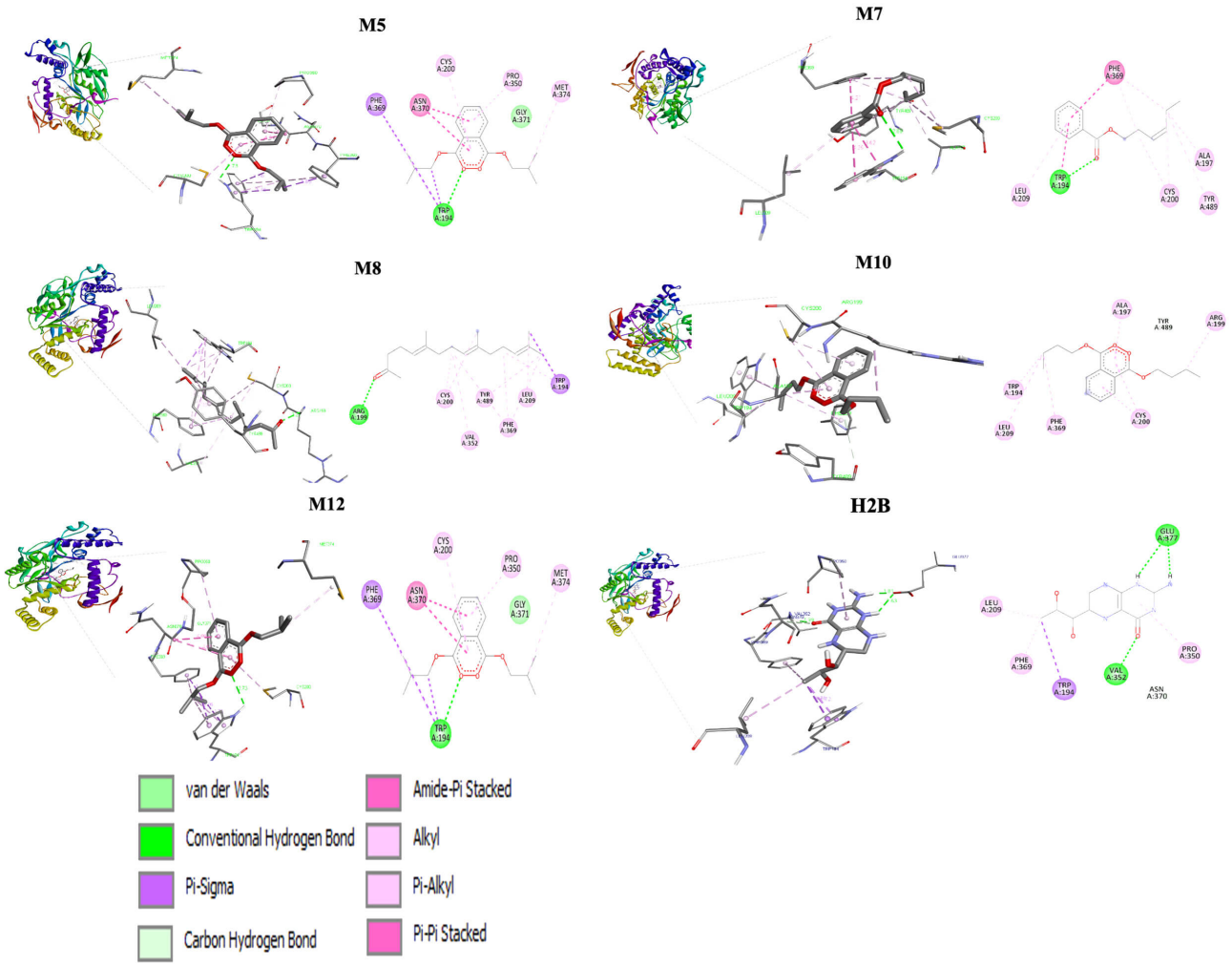

Fig. 3. The 2D and 3D molecular interactions of the most prevalent selected compounds: M5, M7, M8, M10, and M12 with the co-crystallized ligand "H2B" in the binding site of the NOS protein (PDB: 4NOS).

4. Discussion

In the present work, fourteen chemicals were chosen, as shown in Fig. 1C, with relative abundances surpassing 0.5% for computational screening against molecular targets linked with RA. This selection criterion prioritized the major constituents with higher relative abundance and a greater likelihood of contributing to the biological and pharmacological properties of the essential oil, while reducing the influence of trace compounds with limited quantitative significance. The essential oil constituents of parts of *C. spinosa* have been studied in a few countries such as Iran (fruit), Italy (leaves), and Croatia (aerial parts) [48,49,50,51]. Moreover, the composition of the essential oil from the aerial parts of the plant has been investigated in Tabuk, Saudi Arabia [52]. Nevertheless, there are some limitations in the study from Tabuk because the sample used was obtained from Tabuk market instead of a wild-growing plants. In addition, the researchers used whole aerial parts without separation of leaves, stems, flowers, and fruits, which led to less specific compositional profiling. Geographical variability is essential in the determination of the chemical composition of plants, especially those used for medicinal purposes. Plant growth conditions are influenced by environmental factors such as climate, soil composition, altitude, and local biodiversity, resulting in variations in the synthesis of secondary metabolites that contribute to medicinal properties [53]. When faced with environmental stressors such as high temperatures and drought, flora in dry areas may generate greater amounts of certain substances to bolster their protection against herbivores and pathogens [54]. Moreover, variations in soil nutrients influence the concentrations of essential oils, flavonoids, and alkaloids in plant populations from different geographical areas [55,56]. Consequently, these variations exert considerable effects on the effectiveness, safety, and therapeutic potential of medicinal plants. These factors underscore the importance of considering the local environment in pharmacological studies on medicinal plants.

Poor pharmacokinetic properties encompassing ADMET undermine effective pharmaceutical efficacy. More-

Table 8. Docking outcomes of major selected compounds in the essential oil from *C. spinosa* leaves and co-crystallized ligand against TNF-α protein (PDB: 2AZ5).

Ligand	Hydrogen bonds (Distance Å)	Hydrophobic interaction (Distance Å)	Electrostatic and Others (Distance Å)
307	Conventional Hydrogen Bond; Halogen: SC HDO H TYR151 to F (1.43)	π–Sigma: LEU57, TYR119, TYR119 (3.73, 3.93, 3.98) π–π–Stacked: TYR119 (4.18) π–Alkyl: TYR119, TYR119, TYR151, LEU57 (4.83, 4.94, 4.80, 5.05)	Halogen (Fluorine): SER60, SER60, SER60, GLN61 (2.41, 3.59, 2.89, 3.36)
M1	Conventional Hydrogen Bond: BB HDO -NH SER60 to C-O (2.85)	Alkyl: LEU57, LEU57 (5.48, 4.94) π–Alkyl: TYR119, TYR151(4.86, 5.26)	
M5	Conventional Hydrogen Bond: BB HDO -CH GLY121 to C-O (3.25)	π–Sigma: TYR119 (3.60) π–π–Stacked: TYR119 (5.56) π–Alkyl: TYR119, (4.39)	
M7	Conventional Hydrogen Bond: BB HDO -NH GLY121 to C=O (3.00) SC HDO -OH TYR151 to C=O (2.40)	π–Sigma: TYR59 (3.71) π–π Stacked: TYR119 (4.74)	
M8	Conventional Hydrogen Bond: SC HDO -OH TYR151 to C=O (2.09)	Alkyl: LEU57 (4.26) π–Alkyl: TYR119, TYR151(4.89, 5.22)	
M10	Conventional Hydrogen Bond: BB HAC C=O GLY121 to -CH (3.39)	π–π Stacked: TYR119 (4.53) π–π T-shaped: TYR119 (5.58) Amide–π Stacked: TYR119 (5.30) π–Alkyl: TYR119, TYR151 (5.02, 4.85)	
M12	Conventional Hydrogen Bond: BB HDO -NH GLY121 to C=O (2.91) SC HDO -OH TYR151 to C=O (2.40)	π–Sigma: TYR119(3.73) π–Alkyl: TYR119 (4.67)	

Active site (PDB: 2AZ5): LEU57, SER60, TYR119, LEU120, GLY121, GLY122, TYR151. BB, Backbone atoms; SC, Side chain atoms; HDO, H bound donor; HAC, H bound acceptor.

over, unfavorable pharmacokinetics and toxicity are major factors that contribute to the expenses associated with the failure of drug discovery throughout the clinical phase [57]. The ADMET properties of the essential oil from *C. spinosa* leaves were evaluated by *in silico* methods to determine its viability as a therapeutic candidate.

The drug-likeness potential of a high-yield isolated chemical molecule is evaluated using Lipinski's "rule of five". Compounds that exhibit ≥2 violations of Lipinski's rule are identified as possessing insufficient absorbability and permeability, resulting in their exclusion from future drug development [58,59]. MW reflects the size, penetrability, distribution, and uptake potential of a molecule [29]. The LogP value is the most effective measure for evaluating the hydrophobicity of a compound [29]. Furthermore, the number of HDO and HAC bonds reflects the effectiveness of a compound in creating hydrogen bonds to enhance its interactions and stability inside the active site of the target protein [29]. Solubility in water greatly affects absorption rates. When solubility and dissolution rates are low, a drug distributed enterally is likely to be predominantly excreted [60]. The Veber rule evaluates oral bioavailability based primarily on TPSA and the number of rotatable bonds. Drugs that exhibit good oral bioavailability and passive absorption possess TPSA values less than 75 $Å^2$ [61]. The raised values of RBs disrupt penetration rate, thereby reducing oral bioavailability. Decreased RBs (less molecular flexibility) and lower TPSA or HDO and HAC counts indicate favorable oral bioavailability [62]. The acceptable range of MR is recognized to be between 40 and 130. MR serves as a measure of the molecular polarizability [63,64]. The physicochemical study indicated that all the 14 compounds complied with the Lipinski and Vaber criteria. However, compound M2 violated one criterion of Lipinski and one criterion of Veber: LogP ≥5 and 24 rotatable bonds. Furthermore, M2 had poor solubility in water and a high MR. Consequently, except for M2, all other compounds exhibited acceptable drug-like properties.

Skin permeability is a pharmacokinetic indicator that dictates the rate and magnitude of drug absorption via the skin. Thus, elucidating skin permeability is essential for the advancement of transdermal drug delivery approaches [34]. All compounds in this study, except for M2, indicate effective transdermal permeability. The results obtained revealed that all drug candidates, excluding M2, were predicted not to be substrates for P-glycoprotein. This indicates that the compounds would remain unaffected by the efflux activity of P-gp which removes substances from cells, leading to ineffective treatment due to lower drug concentrations than anticipated in plasma and tissues [65,66].

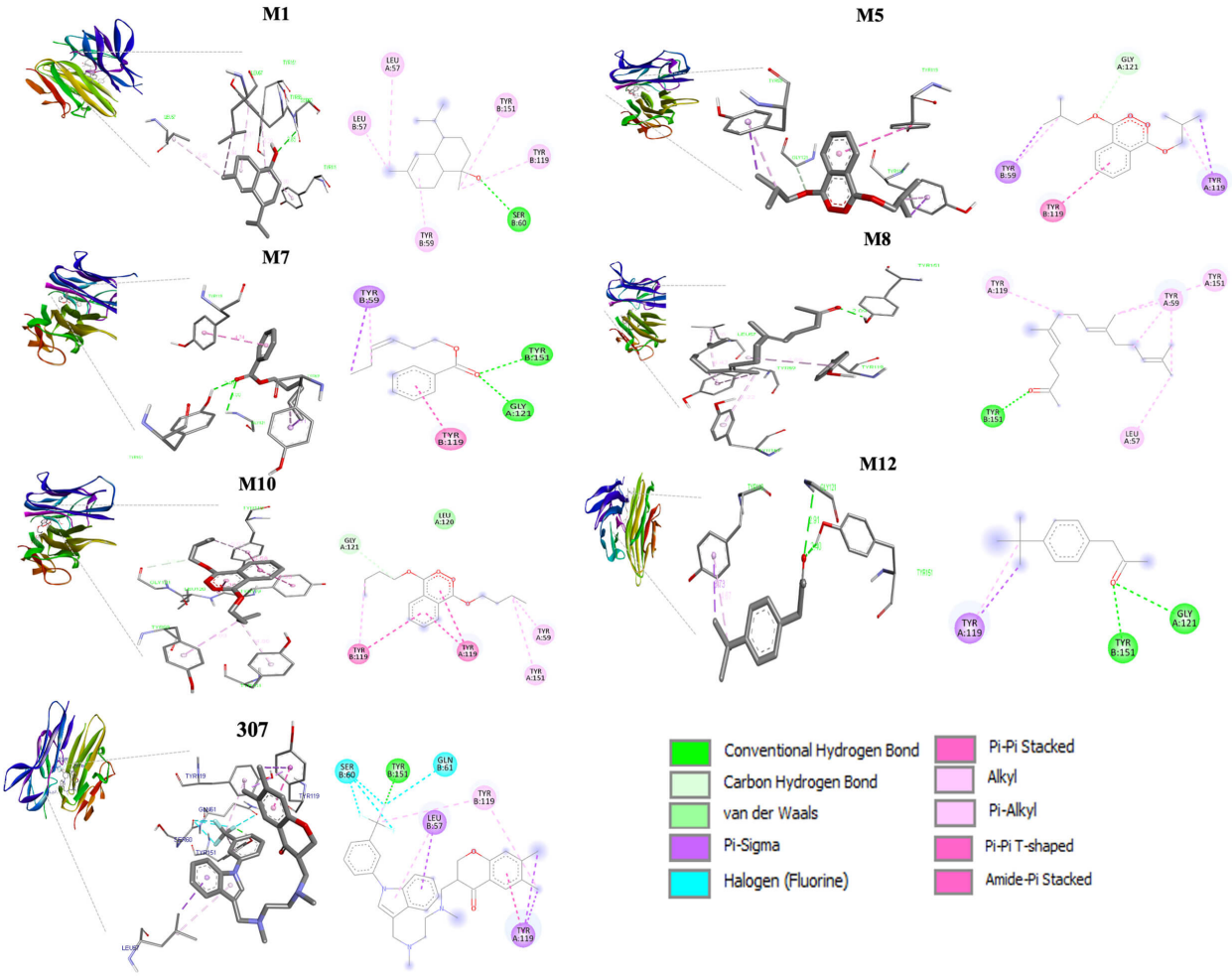

Fig. 4. The 2D and 3D molecular interactions of the most prevalent selected compounds: M1, M5, M7, M8, M10, and M12 with the co-crystallized ligand "307" in the binding site of the TNF-α protein (PDB: 2AZ5).

On the other hand, the results reveal that compounds M2 and M13 were linked to poor intestinal absorption, whereas the remaining compounds had excellent intestinal absorption. Enhanced GI absorption suggests that the compounds will be effectively absorbed from the GI tract post-oral administration [67]. Therefore, M2 had a high proprietary value as P-gp substrate; it was unable to penetrate the dermal skin, and its poor GI absorption further disqualifies it as a drug candidate.

The VDss values for M11 and M14 were low, although M12 and M13 were slightly higher than the recommended range; M4 had the highest VDss value. A very low VDss value signifies that a drug is very likely to reside in the plasma, thereby necessitating a low dosage to achieve the target plasma concentration [68]. This may be a result of a high degree of solubility in water or high affinity for plasma proteins [69]. A high VDss value signifies that a substance will readily be translocated from the plasma into the extravascular space, thereby requiring a large dosage to reach the required plasma concentration [69]. This elevation in VDss is generally related to the binding of drugs to tissue or a high degree of lipid solubility [69]. The BBB acts as a selective filter by restricting the entry of substances into the CNS [70]. The BBB penetration profiles of compounds provide important insights into their probable pharmaceutical impact on the brain or CNS. The molecules M1, M3−M7, M10, and M12 exhibited BBB permeability, indicating potential distribution into the central nervous system. Although this property may support pharmacological activity, it may also raise concerns regarding unintended CNS exposure and possible adverse neurological effects, which should be carefully considered during future drug development and safety evaluation. In contrast, the ligands M2, M8, M9, M11, M13, and M14 exhibited poor capacity to pass through the BBB, indicating their unsuitable distribution in the brain. Nonetheless, this may raise concerns regarding potential CNS-related adverse effects. However, as the computational method fails to quantify the amount of penetration, the degree of penetration might not be substantial enough to predict noticeable toxic effects on the CNS [71].

Table 9. Docking outcomes of major selected compounds in the essential oil from *C. spinosa* leaves and co-crystallized ligand against IL-6 protein (PDB: 1ALU).

Ligand	Hydrogen bonds (Distance Å)	Hydrophobic interaction (Distance Å)
TLA	Conventional Hydrogen Bond: SC HDO: O-H SER22 to C-O (2.62) BB HDO: C=O MET184 to -OH (2.11) BB HAC: C=O ARG182 to -OH (2.35) BB HAC: C=O LEU181 to -OH (2.62)	
M1	-	-
M5	Conventional Hydrogen Bond: SC HDO: -NH ARG30 to C=O (2.88)	π−Sigma: LEU33 (3.89) Alkyl: LEU178 (4.83) π−Alkyl: ARG30, LEU33 (4.36, 4.86)
M7	Conventional Hydrogen Bond: BB HDO -NH GLN175 to C=O (2.74)	π−Sigma: LEU33 (3.67) Alkyl: LEU178, LEU178, ARG182 (4.60, 3.87, 4.36) π−Alkyl: ARG30 (5.02)
M8	Conventional Hydrogen Bond: SC HDO: -NH ARG179 to C=O (2.15) SC HDO: -NH ARG182 to C=O (2.35) SC HDO: CH ARG182 to C=O (1.80)	Alkyl: LYS171, LEU178, LEU33, LEU33, ILE36, LYS171, LYS171 (4.99, 4.82, 4.03, 4.15, 4.57, 3.53, 4.76)
M10	Conventional Hydrogen Bond: BB HAC: C=O LEU33 to -CH (3.30)	π−Sigma: LEU33 (3.84) Alkyl: LEU33, LEU36, LYS171, LEU178, LEU179, (5.07, 4.52, 3.55, 4.86, 4.96) π−Alkyl: ARG30, LEU33 (4.54, 4.60)
M12	Conventional Hydrogen Bond: SC HDO -NH ARG179 to C=O (1.88)	π−Sigma: LEU178 (3.34) Alkyl: LEU33 (4.83)

Active site (PDB: 1ALU): GLN 175, LEU 178, ARG 179, ARG 182. BB, Backbone atoms; SC, Side chain atoms; HDO, H bound donor; HAC, H bound acceptor.

CYP450 enzymes play a central role in phase I drug metabolism and pharmacokinetic drug–drug interactions [72]. The primary mechanisms in pharmacokinetic drug-drug interactions center on the activation of CYP450 enzymes which metabolize 90% of current drugs [72]. Moreover, inhibition of isoforms of this enzymatic system by pharmaceuticals may lead to inadequate excretion, thereby causing drug-induced toxicity. As a result, it is critical for a potential medication to exhibit limited inhibitory effects on CYP450 isoforms [71]. The potential to inhibit 2 isoforms of CYP450 was identified for M5, M7, M8, M10, while M1, M3, M4, M12 and M13 had a tendency to inhibit 1 isoform of CYP450. These predicted inhibitory effects may disrupt normal drug metabolism and increase the risk of pharmacokinetic interactions and compound accumulation, highlighting potential safety considerations for future drug development. However, compounds M2, M6, M9, M11, and M14 did not show potential for an inhibitory effect on any of the CYP450 isoforms. Furthermore, the predictive toxicity analysis identified six compounds within Toxicity Classes 5 and 6. Although several compounds demonstrated favorable pharmacokinetic and docking profiles, the predicted toxicological liabilities warrant careful safety evaluation and further *in vitro* and *in vivo* validation before considering potential therapeutic applications.

Computational approaches have become increasingly important in modern drug discovery by facilitating rapid screening of bioactive compounds and reducing the time and cost associated with therapeutic development [73]. Among these approaches, molecular docking plays a key role in predicting ligand–target interactions and identifying compounds with potential pharmacological relevance. In this context, natural products represent valuable sources of structurally diverse bioactive molecules with potential anti-inflammatory and therapeutic applications [74]. Accordingly, the present study employed molecular docking analysis to investigate the predicted interactions of major phytochemicals identified in the essential oil of *C. spinosa* with RA-associated molecular targets. Virtual screening methods are often employed to reduce the expenses and shorten the duration associated with drug development. Molecular docking, a technique employed to identify novel ligands for

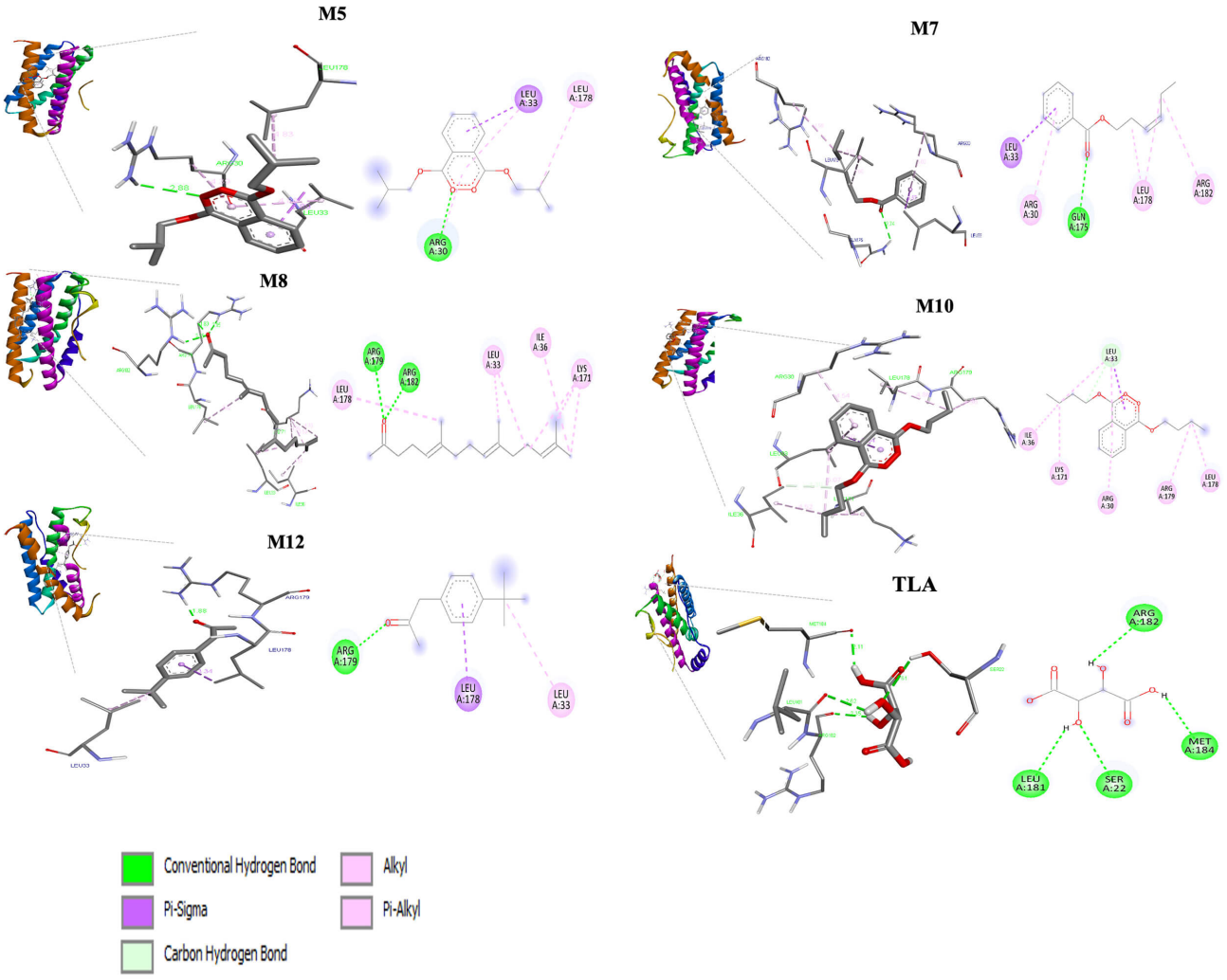

Fig. 5. The 2D and 3D molecular interactions of the most prevalent selected compounds: M5, M7, M8, M10, and M12 with the co-crystallized ligand "TLA" in the binding site of the IL-6 protein (PDB: 1ALU).

protein structures, is critical in structure-based drug design. The interaction between a compound and the receptor is crucial in drug formulation [73]. Natural products have the potential to mitigate a diverse range of human diseases such as cancer and inflammation. Numerous medications are sourced from these natural compounds. For instance, the anticancer agent paclitaxel (taxol) is obtained from extracts of Taxus brevifolia. Plant-based medicines present promising alternatives to modern drugs, especially considering the increasing drug resistance observed in numerous diseases, along with the minimal side effects associated with plant-derived treatments [74].

RA is initially characterized by persistent cellular activation which leads to autoimmunity in the joints or other organs [4,75,76]. The clinical signs of the condition arise mainly after synovial inflammation and joint damage. Fibroblast-like synoviocytes (FLS) are critical to these pathogenic processes [77,78,79]. The disease progresses through three stages: an initial, non-specific inflammatory phase that is exacerbated by T-cell activation in the synovium; a chronic inflammatory phase; and a tissue damage phase that is mediated by cytokines such as IL-1, IL-6, and TNF-α [4,80,81,82,83]. The activation of innate immunity progresses in a stepwise manner under specific environmental or genetic influences [4]. This process begins with the stimulation of dendritic cells, which subsequently recruit and activate T cells [4]. Then, these T cells stimulate B cells, macrophages, synoviocytes, chondrocytes, and osteoclasts to secrete pro-inflammatory and bone-resorbing cytokines such as IL-1β, IL-6, TNF-α, and matrix metalloproteinases (MMPs). This cascade results in damage to bone and cartilage, in association with thickening of synovial membranes and angiogenesis in the synovium and adjacent bone marrow [4]. The combination of adaptive and innate immune pathways, which facilitate tissue remodeling and damage, is a driving factor in the chronic phase of RA. Drugs targeting inflammatory cytokine signaling are frequently utilized in clinical practice [4].

Table 10. Docking outcomes of major selected compounds in the essential oil from *C. spinosa* leaves and co-crystallized ligand against the cyclooxygenase-2 protein (PDB: 5F1A).

Ligand	Hydrogen bonds (Distance Å)	Hydrophobic interaction (Distance Å)
COH	Conventional Hydrogen Bond: SC HAC: N HIS214 to -OH (2.63) SC HAC: O THR212 to -OH (2.41)	π–π T-shaped: HIS207 (4.38) Alkyl: ALA202, VAL295, LEU391, LEU294, LEU294, VAL295, ILE408, LEU390, LEU391 (3.56, 3.61, 4.68, 5.28, 4.57, 4.96, 5.33, 4.78, 4.40) π–Alkyl: PHE200, TRP387, PHE395, LEU391, HIS207, PHE210, HIS386 (4.83, 5.26, 5.42, 5.06, 5.17, 5.08, 4.30)
SAL	Conventional Hydrogen Bond: SC HDO: -NH HIS388 to C=O (2.39)	Amide–π Stacked: TRP387 (4.21) π–Alkyl: ALA202, LEU390 (5.11, 5.06)
M1	Conventional Hydrogen Bond: SC HDO: -NH HIS388 to C-O (1.90)	Alkyl: ALA202, LEU391 (4.21, 4.60) π–Alkyl: HIS207, HIS207, HIS386, HIS386, HIS388 (4.80, 4.81, 5.25, 4.15, 5.35)
M5	Conventional Hydrogen Bond: SC HDO: -NH HIS388 to C-O (2.39)	π–π T-shaped: HIS207 (4.63) Alkyl: LEU390, LEU391 (4.90, 4.47) π–Alkyl: HIS386 (4.19)
M7	Conventional Hydrogen Bond: BB HDO: -NH TRP387 to C=O (2.80) SC HDO: -NH HIS388 to C=O (2.41)	Alkyl: LEU391 (4.64) π–Alkyl: ALA202 (4.88)
M8	-	π–Sigma: HIS386 (3.80) Alkyl: ALA202, LEU391, LEU391, VAL295, ILE408, LEU294, VAL295, ILE408 (4.33, 4.17, 4.53, 4.00, 5.42, 4.14, 4.29, 4.70) π–Alkyl: HIS207, TRP387, PHE395, TYR404 (5.36, 5.20, 4.89, 4.78)
M10	Conventional Hydrogen Bond: BB HDO: -NH TRP387 to C-O (2.89) SC HDO: -NH HIS388 to C=O (2.37)	Alkyl: VAL295, LEU391 (3.86, 4.51) π–Alkyl: PHE200, HIS207, HIS386, ALA202, LEU391, LEU391 (5.38, 4.91, 4.46, 5.50, 5.49, 5.24)
M12	Conventional Hydrogen Bond: SC HDO: -NH HIS388 to C=O (2.38)	Alkyl: VAL295, LEU391 (4.97, 4.66) π–Alkyl: LEU391 (4.76)

Active site (PDB: 5FLA): TYR148, ALA199, PHE200, ALA202, GLN203, THR206, HIS207, PHE210, LYS211, THR212, ASP213, HIE214, ASN222, GLN289, VAL291, ASN382, TYR385, HIE386, TRP387, HIE388, LUE390, LUE391 and VAL447. BB, Backbone atoms; SC, Side chain atoms; HDO, H bound donor; HAC, H bound acceptor.

Extensive mechanistic investigations have established that RA is a chronic inflammatory condition marked by the activation of mitogen-activated protein kinases (MAPKs), particularly extracellular signal-regulated kinase (ERK), c-Jun N-terminal kinase (JNK), and p38, which play crucial roles in the activation of nuclear factor κ-B (NF-κB), a protein complex that regulates DNA transcription, cytokine production, and cellular survival functions [84,85]. Elevated activity of the MAPK signaling pathway might enhance the secretion of proinflammatory mediators such as TNF-α, IL-6, IL-1β, NO, iNOS, and COX-2. Consequently, joint damage and joint dysfunction occur, thereby further aggravating the pathology of arthritis and intensifying symptoms like joint pain, swelling, and functional impairment in patients [86,87,88,89]. Emerging evidence indicates that the decoction of *Fangji Huangqi* reduced levels of reactive oxygen species and NO in a concentration-dependent manner in lipopolysaccharide (LPS)-stimulated

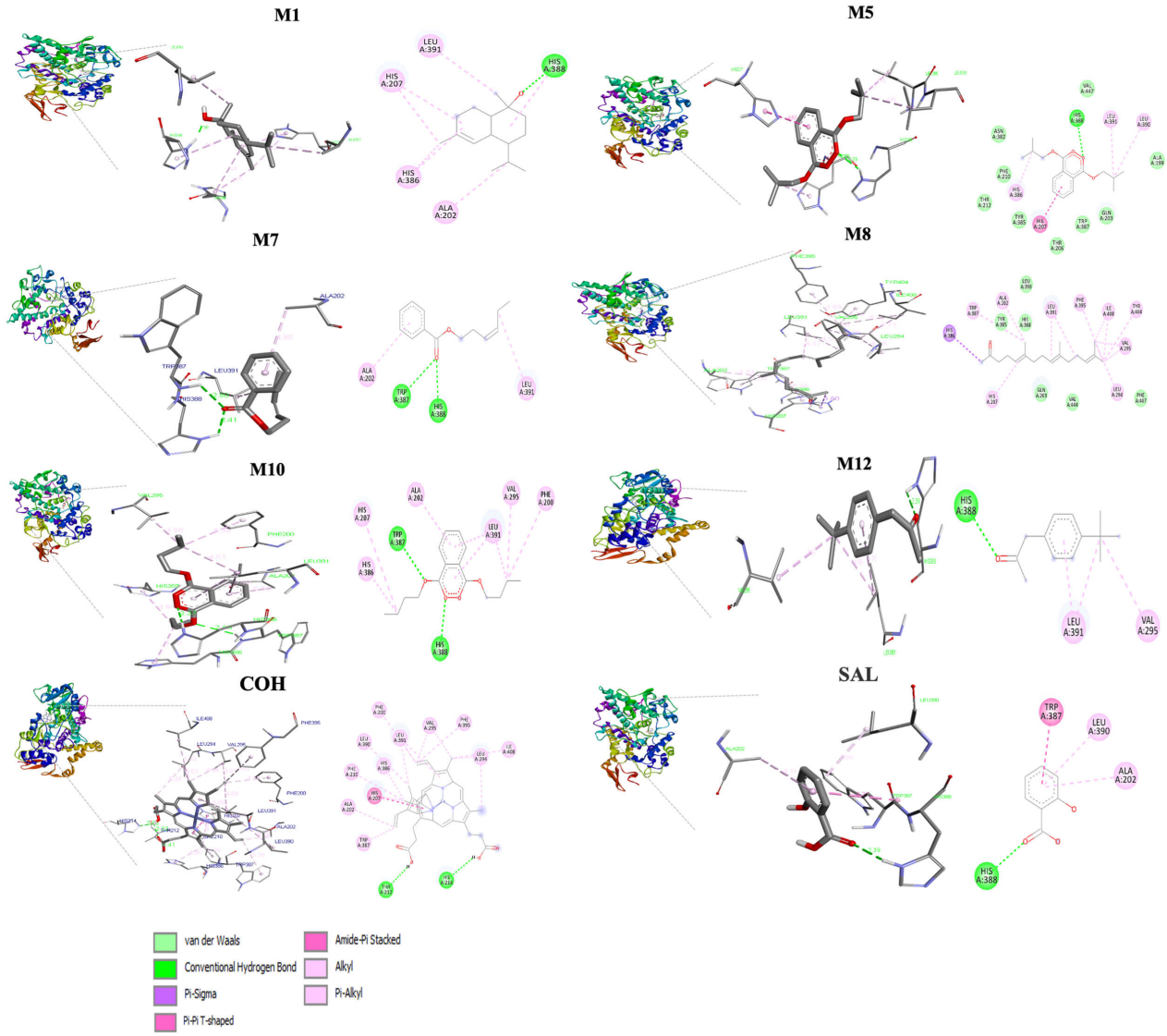

Fig. 6. The 2D and 3D molecular interactions of the most prevalent selected compounds: M1, M5, M7, M8, M10, and M12 with the co-crystallized ligands "COH & SAL" in the binding site of cyclooxygenase-2 protein (PDB: 5F1A).

RAW264.7 cells. Additionally, it lowered levels of iNOS, COX-2, TNF-α, IL-1β, IL-6, and phosphorylated protein forms of p38, ERK, JNK, and NF-κB p65 [90].

This study involved a molecular docking analysis aimed at examining the predicted binding affinities of major phytochemicals derived from the essential oil of *C. spinosa* with the proteins IL-1β, NOS, TNF-α, IL-6, and COX-2, as computationally relevant RA-associated targets. Diisobutyl phthalate (M5) exhibited best binding energy scores against IL-1β and NOS compared to other compounds and co-crystallized ligands. Given that IL-1β is remarkably correlated to synovial inflammation and tissue damage [4], whereas iNOS plays a role in nitric oxide-mediated inflammatory and oxidative stress pathways [6], the identified interactions may indicate a potential modulation of RA-linked signaling mechanisms under the predicted computational conditions.

Tau-cadinol (M1) indicated the highest binding energy for TNF-α among the investigated phytochemicals. Since TNF-α plays a pivotal role as a cytokine involved in promoting inflammation, it may lead to chronic inflammation and tissue damage [4]. The predicted interaction of tau-cadinol with TNF-α suggests its potential as a candidate for regulating cytokine-driven inflammatory responses correlated with RA progression.

Six prominent phytochemicals, tau-cadinol (M1), diisobutyl phthalate (M5), (Z)-3-hexenyl benzoate (M7), farnesyl acetone (M8), dibutyl phthalate (M10), and 1-(4-tert-butylphenyl)propan-2-one (M12), displayed notably favorable docking affinities for IL-6 and COX-2, with M10 exhibiting the lowest docking energy values among the evaluated compounds under the applied computational conditions. Considering the previously demonstrated functions of IL-6 in chronic inflammation and COX-2 in

prostaglandin-mediated inflammatory responses [4], these findings further highlight the potential relevance of the identified compounds as desirable candidates for further exploration against RA-related inflammatory targets.

5. Limitations

This study represents a preliminary computational investigation exploring the predicted pharmacological relevance of compounds identified in the essential oil of *Capparis spinosa* L. against rheumatoid arthritis–associated molecular targets through the integration of GC-MS analysis, ADME prediction, and molecular docking approaches. The findings provide initial insights into the potential interactions between the identified phytochemicals and selected inflammatory protein targets, supporting the potential scientific relevance of *C. spinosa* as a natural source of bioactive compounds. Although the current results are exploratory and computational in nature, they may provide a useful foundation for future experimental and pharmacological investigations aimed at validating the biological activity and therapeutic relevance of these compounds in more complex biological systems. Another limitation of the current research is the absence of a deposited herbarium voucher specimen at the period of plant collection; hence, a voucher specimen number is unavailable. The collection region, including geographic coordinates, alongside a taxonomic verification by a plant taxonomy specialist, has been provided to enhance the documentation and traceability of the plant material utilized in this study. A constraint of this research is that plant collection, essential oil extraction, and GC-MS analysis were conducted just once with a singular sample, lacking independent repetitions. Consequently, the results reflect the examined sample, and their replicability and applicability should be regarded with caution.

6. Conclusion

In the current investigation, GC-MS was used to identify bioactive substances derived from the essential oil of *C. spinosa* leaves. Molecular docking studies were carried out on the proteins TNF-α (PDB: 2AZ5), IL-6 (PDB: 1ALU), IL-1β (PDB: 5R8Q), NOS (PDB: 4NOS), and COX-2 (PDB: 5F1A) in order to unravel possible novel targets for RA derived from the most abundant compounds identified in *C. spinosa* leaf essential oil. All compounds that exhibited unsuitable ADMET characteristics were excluded. Six candidates were identified as having favorable ADMET profiles: tau-cadinol (M1), diisobutyl phthalate (M5), (Z)-3-hexenyl benzoate (M7), farnesyl acetone (M8), dibutyl phthalate (M10), and 1-(4-tert-butylphenyl) propan-2-one (M12). The present findings provide preliminary computational insights into the possible interactions between selected phytochemicals and RA-related molecular targets. Nevertheless, future studies involving molecular dynamics simulations, *in vitro* assays, and *in vivo* experimental models are necessary to validate the biological relevance, safety, and therapeutic feasibility of the reported compounds.

Availability of Data and Materials

The original contributions from this study are provided in the article. Any further inquiries can be directed to the corresponding author.

Author Contributions

SA and WA designed the research study. SA and WA performed the research. SA and WA analyzed the data. SA and WA wrote the manuscript. Both authors contributed to editorial changes in the manuscript. Both authors read and approved the final manuscript. Both authors have participated sufficiently in the work and agreed to be accountable for all aspects of the work.

Ethics Approval and Consent to Participate

Not applicable.

Acknowledgment

Thanks to all the peer reviewers for their opinions and suggestions.

Funding

This research received no external funding.

Conflicts of Interest

The authors declare no conflicts of interest.

Supplementary Material

Supplementary material associated with this article can be found in the online version, at https://doi.org/10.31083/Pharmazie52565.

References

[1] Huang J, Fu X, Chen X, Li Z, Huang Y, Liang C. Promising Therapeutic Targets for Treatment of Rheumatoid Arthritis. Frontiers in Immunology. 2021; 12: 686155. https://doi.org/10.3389/fimmu.2021.686155

[2] Firestein GS. Evolving concepts of rheumatoid arthritis. Nature. 2003; 423: 356–361. https://doi.org/10.1038/nature01661

[3] Ngo ST, Steyn FJ, McCombe PA. Gender differences in autoimmune disease. Frontiers in Neuroendocrinology. 2014; 35: 347–369. https://doi.org/10.1016/j.yfrne.2014.04.004

[4] Ding Q, Hu W, Wang R, Yang Q, Zhu M, Li M, et al. Signaling pathways in rheumatoid arthritis: implications for targeted therapy. Signal Transduction and Targeted Therapy. 2023; 8: 68. https://doi.org/10.1038/s41392-023-01331-9

[5] Sharma D, Chaubey P, Suvarna V. Role of natural products in alleviation of rheumatoid arthritis-A review. Journal of Food Biochemistry. 2021; 45: e13673. https://doi.org/10.1111/jfbc.13673

[6] Huang JB, Chen ZR, Yang SL, Hong FF. Nitric Oxide Synthases in Rheumatoid Arthritis. Molecules (Basel, Switzerland). 2023; 28: 4414. https://doi.org/10.3390/molecules28114414

[7] Hamim SI, Roney M, Uddin MN, Issahaku AR, Chhando KS, Aluwi MF, et al. Investigating the potential compounds of Kalanchoe pinnata plant for the treatment of Inflammation utilizing molecular docking and molecular dynamic simulation approach. In Silico Research in Biomedicine. 2025; 1: 100007. https://doi.org/10.1016/j.insi.2025.100007

[8] Refaey MS, Abouelela ME, El-Shoura EAM, Alkhalidi HM, Fadil SA, Elhady SS, et al. In Vitro Anti-Inflammatory Activity of *Cotula anthemoides* Essential Oil and In Silico Molecular Docking of Its Bioactives. Molecules (Basel, Switzerland). 2022; 27: 1994. https://doi.org/10.3390/molecules27061994

[9] Islam MA, Zilani MNH, Biswas P, Khan DA, Rahman MH, Nahid R, et al. Evaluation of in vitro and in silico anti-inflammatory potential of some selected medicinal plants of Bangladesh against cyclooxygenase-II enzyme. Journal of Ethnopharmacology. 2022; 285: 114900. https://doi.org/10.1016/j.jep.2021.114900

[10] Annaz H, Sane Y, Bitchagno GTM, Ben Bakrim W, Drissi B, Mahdi I, et al. Caper (*Capparis spinosa* L.): An Updated Review on Its Phytochemistry, Nutritional Value, Traditional Uses, and Therapeutic Potential. Frontiers in Pharmacology. 2022; 13: 878749. https://doi.org/10.3389/fphar.2022.878749

[11] Sun Y, Yang T, Wang C. Capparis spinosa L. as a potential source of nutrition and its health benefits in foods: A comprehensive review of its phytochemistry, bioactivities, safety, and application. Food Chemistry. 2023; 409: 135258. https://doi.org/10.1016/j.foodchem.2022.135258

[12] Zhang S, Liu K, Liu Y, Hu X, Gu X. The role and application of bioinformatics techniques and tools in drug discovery. Frontiers in Pharmacology. 2025; 16: 1547131. https://doi.org/10.3389/fphar.2025.1547131

[13] Srinivasan P, Vijayakumar S, Kothandaraman S, Palani M. Anti-diabetic activity of quercetin extracted from *Phyllanthus emblica* L. fruit: *In silico* and *in vivo* approaches. Journal of Pharmaceutical Analysis. 2018; 8: 109–118. https://doi.org/10.1016/j.jpha.2017.10.005

[14] Wu F, Zhou Y, Li L, Shen X, Chen G, Wang X, et al. Computational Approaches in Preclinical Studies on Drug Discovery and Development. Frontiers in Chemistry. 2020; 8: 726. https://doi.org/10.3389/fchem.2020.00726

[15] Kim S, Chen J, Cheng T, Gindulyte A, He J, He S, et al. PubChem 2019 update: improved access to chemical data. Nucleic Acids Research. 2019; 47: D1102–D1109. https://doi.org/10.1093/nar/gky1033

[16] Singh DB, Gupta MK, Singh DV, Singh SK, Misra K. Docking and in silico ADMET studies of noraristeromycin, curcumin and its derivatives with Plasmodium falciparum SAH hydrolase: a molecular drug target against malaria. Interdisciplinary Sciences, Computational Life Sciences. 2013; 5: 1–12. https://doi.org/10.1007/s12539-013-0147-z

[17] da Silva CPM, das Neves GM, Poser GLV, Eifler-Lima VL, Rates SMK. In silico Prediction of ADMET/Drug-likeness Properties of Bioactive Phloroglucinols from Hypericum Genus. Medicinal chemistry (Shariqah (United Arab Emirates)), 19, 1002–1017. https://doi.org/10.2174/1573406419666230601092358

[18] Azzam KA. SwissADME and pkCSM webservers predictors: An integrated online platform for accurate and comprehensive predictions for in silico ADME/T properties of artemisinin and its derivatives. Kompleksnoe Ispolzovanie Mineralnogo Syra= Complex use of mineral resources. 2023; 325: 14–21. https://doi.org/10.31643/2023/6445.13

[19] Daina A, Michielin O, Zoete V. SwissADME: a free web tool to evaluate pharmacokinetics, drug-likeness and medicinal chemistry friendliness of small molecules. Scientific Reports. 2017; 7: 42717. https://doi.org/10.1038/srep42717

[20] Lipinski CA. Lead- and drug-like compounds: the rule-of-five revolution. Drug Discovery Today. Technologies. 2004; 1: 337–341. https://doi.org/10.1016/j.ddtec.2004.11.007

[21] Khan MTH. Predictions of the ADMET properties of candidate drug molecules utilizing different QSAR/QSPR modelling approaches. Current Drug Metabolism. 2010; 11: 285–295. https://doi.org/10.2174/138920010791514306

[22] Kim S, Thiessen PA, Cheng T, Yu B, Bolton EE. An update on PUG-REST: RESTful interface for programmatic access to PubChem.Nucleic Acids Research, 2018; 46: W563-W570.https://doi.org/10.1093/nar/gky294

[23] Berman HM, Westbrook J, Feng Z, Gilliland G, Bhat TN, Weissig H, et al. The Protein Data Bank. Nucleic Acids Research. 2000; 28: 235–242. https://doi.org/10.1093/nar/28.1.235

[24] Hasan MM, Khan Z, Chowdhury MS, Khan MA, Moni MA, Rahman MH. In silico molecular docking and ADME/T analysis of Quercetin compound with its evaluation of broad-spectrum therapeutic potential against particular diseases. Informatics in Medicine Unlocked. 2022; 29: 100894. https://doi.org/10.1016/j.imu.2022.100894

[25] Gorgulla C, Jayaraj A, Fackeldey K, Arthanari H. Emerging frontiers in virtual drug discovery: From quantum mechanical methods to deep learning approaches. Current Opinion in Chemical Biology, 2022;69:102156. https://doi.org/10.1016/j.cbpa.2022.102156

[26] Trott O, Olson AJ. AutoDock Vina: improving the speed and accuracy of docking with a new scoring function, efficient optimization, and multithreading. Journal of Computational Chemistry. 2010; 31: 455–461. https://doi.org/10.1002/jcc.21334

[27] Joshi KR, Devkota HP, Al-Mutairi KA, Sugimura K, Yahara S, Khadka R, et al. Therapeutic potential of Leea asiatica: Chemical isolation and validation of ethnomedicinal claims through in vitro and in silico assessment of antioxidant and anti-inflammatory properties. Heliyon. 2024;10:e38074. https://doi.org/10.1016/j.heliyon.2024.e38074

[28] Beura S, Chetti P. Identification of potential human COX-2 inhibitors using computational modeling and molecular dynamics simulations. Journal of Molecular Structure. 2020; 1216: 128271. https://doi.org/10.1016/j.molstruc.2020.128271

[29] Baccari W, Saidi I, Filali I, Znati M, Tounsi M, Ascrizzi R, et al. The root essential oil from the Tunisian endemic plant Ferula tunetana: Chemical composition, biological evaluation, molecular docking analysis and drug-likeness prediction. Arabian Journal of Chemistry. 2023; 16: 105044.

[30] Di L, Kerns EH. Solution stability–plasma, gastrointestinal, bioassay. Current Drug Metabolism. 2008; 9: 860–868. https://doi.org/10.2174/138920008786485218

[31] Vlad IM, Nuta DC, Chirita C, Caproiu MT, Draghici C, Dumitrascu F, et al. In silico and in vitro experimental studies of new dibenz [b, e] oxepin-11 (6 H) one O-(arylcarbamoyl)-oximes designed as potential antimicrobial agents. Molecules. 2020; 25: 321. https://doi.org/10.3390/molecules25020321

[32] Kumari A, kumar R, Sulabh G, Singh P, Kumar J, Singh VK, et al. In silico ADMET, molecular docking and molecular simulation-based study of glabridin's natural and semisynthetic derivatives as potential tyrosinase inhibitors. Advances in Traditional Medicine. 2023; 23: 733–751. https://doi.org/10.1007/s13596-022-00640-8

[33] Ashmawy SM, El-Gizawy SA, El Maghraby GM, Osman MA. Regional difference in intestinal drug absorption as a measure for the potential effect of P-glycoprotein efflux transporters. The Journal of Pharmacy and Pharmacology. 2019; 71: 362–370. https://doi.org/10.1111/jphp.13036

[34] Akili AWR, Hardianto A, Latip J, Permana A, Herlina T. Virtual Screening and ADMET Prediction to Uncover the Potency of Flavonoids from Genus *Erythrina* as Antibacterial

Agent through Inhibition of Bacterial ATPase DNA Gyrase B. Molecules (Basel, Switzerland). 2023; 28: 8010. https://doi.org/10.3390/molecules28248010

[35] Stillhart C, Vučićević K, Augustijns P, Basit AW, Batchelor H, Flanagan TR, et al. Impact of gastrointestinal physiology on drug absorption in special populations–An UNGAP review. European Journal of Pharmaceutical Sciences: Official Journal of the European Federation for Pharmaceutical Sciences. 2020; 147: 105280. https://doi.org/10.1016/j.ejps.2020.105280

[36] Drapak I, Zimenkovsky B, Matiichuk Y, Skrobala V, Kaminskyy D, Oliinyk M, et al. Synthesis, analysis adme-tox parameters and anti-cancer activity of n-(5-r-benzylthiazole-2-yl)-2-morpholin-4-yl-2-thioxoacetamides. Proceeding of the Shevchenko Scientific Society. Medical Sciences. 2024; 73. https://doi.org/10.25040/ntsh2024.01.19

[37] Alahmari, A. Blood-brain barrier overview: Structural and functional correlation. Neural plasticity. 2021: .6564585https://doi.org/10.1155/2021/6564585

[38] Yeni Y, Rachmania RA. The prediction of pharmacokinetic properties of compounds in Hemigraphis alternata (Burm. F.) T. Ander leaves using pkCSM. Indonesian Journal of Chemistry. 2022; 22: 1081–1089. https://doi.org/10.22146/ijc.73117

[39] Bhosle VK, Altit G, Autmizguine J, Chemtob S. Basic pharmacologic principles. Fetal and Neonatal Physiology (pp. 187–201). Elsevier: Philadelphia. 2017.

[40] Klimoszek D, Jeleń M, Dołowy M, Morak-Młodawska B. Study of the Lipophilicity and ADMET Parameters of New Anticancer Diquinothiazines with Pharmacophore Substituents. Pharmaceuticals (Basel, Switzerland). 2024; 17: 725. https://doi.org/10.3390/ph17060725

[41] Thomas DN, Wills JW, Burman M, Williams AN, Harte DSG, Buckley RA, et al. Resolution of historically discordant Ames test negative/rodent carcinogenicity positive N-nitrosamines using a sensitive, OECD-aligned design. Mutagenesis. 2025; 40: 116–125. https://doi.org/10.1093/mutage/geae027

[42] Drwal MN, Banerjee P, Dunkel M, Wettig MR, Preissner R. ProTox: a web server for the in silico prediction of rodent oral toxicity. Nucleic Acids Research. 2014; 42: W53–W58. https://doi.org/10.1093/nar/gku401

[43] Coimbra JTS, Feghali R, Ribeiro RP, Ramos MJ, Fernandes PA. The importance of intramolecular hydrogen bonds on the translocation of the small drug piracetam through a lipid bilayer. RSC Advances. 2021; 11: 899–908. https://doi.org/10.1039/d0ra09995c

[44] Zha X, Ji R, Li Y, Cao R, Zhou S. Network pharmacology, molecular docking, and molecular dynamics simulation analysis reveal the molecular mechanism of halociline against gastric cancer. Molecular Diversity. 2025; 29: 4693–4703. https://doi.org/10.1007/s11030-024-10822-y

[45] Song Y, Sakharkar MK, Yang J. Probing the mechanism of action (MOA) of Solanum nigrum Linn against breast cancer using network pharmacology and molecular docking. SN Applied Sciences. 2023; 5: 133. https://doi.org/10.1007/s42452-023-05356-1

[46] Cole JC, Murray CW, Nissink JWM, Taylor RD, Taylor R. Comparing protein-ligand docking programs is difficult. Proteins. 2005; 60: 325–332. https://doi.org/10.1002/prot.20497

[47] Yuriev E, Ramsland PA. Latest developments in molecular docking: 2010-2011 in review. Journal of Molecular Recognition: JMR. 2013; 26: 215–239. https://doi.org/10.1002/jmr.2266

[48] Kulisic-Bilusic T, Blažević I, Dejanović B, Miloš M, Pifat G. Evaluation of the antioxidant activity of essential oils from caper (Capparis spinosa) and sea fennel (Crithmum maritimum) by different methods. Journal of Food Biochemistry. 2010; 34: 286–302. https://doi.org/10.1111/j.1745-4514.2009.00330.x

[49] Kulisic-Bilusic T, Schmöller I, Schnäbele K, Siracusa L, Ruberto G. The anticarcinogenic potential of essential oil and aqueous infusion from caper (Capparis spinosa L.). Food Chemistry. 2012; 132: 261–267. https://doi.org/10.1016/j.foodchem.2011.10.074

[50] Merlino M, Condurso C, Cincotta F, Nalbone L, Ziino G, Verzera A. Essential Oil Emulsion from Caper (*Capparis spinosa* L.) Leaves: Exploration of Its Antibacterial and Antioxidant Properties for Possible Application as a Natural Food Preservative. Antioxidants (Basel, Switzerland). 2024; 13: 718. https://doi.org/10.3390/antiox13060718

[51] Shafaghi Rad M, Nouri M. Inspection of *Capparis spinosa* essential oils for quality assurance of fish burgers during refrigerated storage. Food Science & Nutrition. 2023; 11: 7229–7241. https://doi.org/10.1002/fsn3.3648

[52] Alkhaibari AM, Alanazi AD. Chemical Composition and Insecticidal, Antiplasmodial, and Anti-Leishmanial Activity of *Capparis spinosa* Essential Oil and Its Main Constituents. Evidence-based Complementary and Alternative Medicine: ECAM. 2022; 2022: 6371274. https://doi.org/10.1155/2022/6371274

[53] Alum EU. Climate change and its impact on the bioactive compound profile of medicinal plants: implications for global health. Plant Signaling & Behavior. 2024; 19: 2419683. https://doi.org/10.1080/15592324.2024.2419683

[54] Saini N, Anmol A, Kumar S, Wani AW, Bakshi M, Dhiman Z. Exploring phenolic compounds as natural stress alleviators in plants-a comprehensive review. Physiological and Molecular Plant Pathology. 2024; 133: 102383. https://doi.org/10.1016/j.pmpp.2024.102383

[55] Pant P, Pandey S, Dall'Acqua S. The Influence of Environmental Conditions on Secondary Metabolites in Medicinal Plants: A Literature Review. Chemistry & Biodiversity. 2021; 18: e2100345. https://doi.org/10.1002/cbdv.202100345

[56] Yang L, Wen KS, Ruan X, Zhao YX, Wei F, Wang Q. Response of Plant Secondary Metabolites to Environmental Factors. Molecules (Basel, Switzerland). 2018; 23: 762. https://doi.org/10.3390/molecules23040762

[57] Kandsi F, Lafdil FZ, Elbouzidi A, Bouknana S, Miry A, Addi M, et al. Evaluation of Acute and Subacute Toxicity and LC-MS/MS Compositional Alkaloid Determination of the Hydroethanolic Extract of *Dysphania ambrosioides* (L.) Mosyakin and Clemants Flowers. Toxins. 2022; 14: 475. https://doi.org/10.3390/toxins14070475

[58] Lipinski CA, Lombardo F, Dominy BW, Feeney PJ. Experimental and computational approaches to estimate solubility and permeability in drug discovery and development settings. Advanced Drug Delivery Reviews. 2001; 46: 3–26. https://doi.org/10.1016/s0169-409x(00)00129-0

[59] Aldahish A, Balaji P, Vasudevan R, Kandasamy G, James JP, Prabahar K. Elucidating the Potential Inhibitor against Type 2 Diabetes Mellitus Associated Gene of GLUT4. Journal of Personalized Medicine. 2023; 13: 660. https://doi.org/10.3390/jpm13040660

[60] Jorgensen WL, Duffy EM. Prediction of drug solubility from structure. Advanced Drug Delivery Reviews. 2002; 54: 355–366. https://doi.org/10.1016/s0169-409x(02)00008-x

[61] Johari NA, Sapi'i NA, Jiunn Hieng AL, Ab Latif N, Amran SI, Hasham R, et al. *In vitro* and *in silico* evaluation of *Andrographis paniculata* ethanolic crude extracts on fatty acid synthase expression on breast cancer cells. BioMedicine. 2024; 14: 60–73. https://doi.org/10.37796/2211-8039.1444

[62] Veber DF, Johnson SR, Cheng HY, Smith BR, Ward KW, Kopple KD. Molecular properties that influence the oral bioavailability of drug candidates. Journal of Medicinal Chemistry. 2002; 45: 2615–2623. https://doi.org/10.1021/jm020017n

[63] Ghose AK, Viswanadhan VN, Wendoloski JJ. A knowledge-based approach in designing combinatorial or medicinal chem-

istry libraries for drug discovery. 1. A qualitative and quantitative characterization of known drug databases. Journal of Combinatorial Chemistry. 1999; 1: 55–68. https://doi.org/10.1021/cc9800071

[64] Verma RP, Hansch C. A comparison between two polarizability parameters in chemical–biological interactions. Bioorganic & Medicinal Chemistry. 2005; 13: 2355–2372. https://doi.org/10.1016/j.bmc.2005.01.051

[65] Kim RB. Drugs as P-glycoprotein substrates, inhibitors, and inducers. Drug Metabolism Reviews. 2002; 34: 47–54. https://doi.org/10.1081/dmr-120001389

[66] Finch A, Pillans P. P-glycoprotein and its role in drug-drug interactions. Australian Prescriber. 2014; 37.

[67] Luo Z, Paunović N, Leroux JC. Physical methods for enhancing drug absorption from the gastrointestinal tract. Advanced Drug Delivery Reviews. 2021; 175: 113814. https://doi.org/10.1016/j.addr.2021.05.024

[68] Smith DA, Beaumont K, Maurer TS, Di L. Volume of Distribution in Drug Design. Journal of Medicinal Chemistry. 2015; 58: 5691–5698. https://doi.org/10.1021/acs.jmedchem.5b00201

[69] Gombar VK, Hall SD. Quantitative structure-activity relationship models of clinical pharmacokinetics: clearance and volume of distribution. Journal of Chemical Information and Modeling. 2013; 53: 948–957. https://doi.org/10.1021/ci400001u

[70] Kiela PR, Ghishan FK. Physiology of Intestinal Absorption and Secretion. Best Practice & Research. Clinical Gastroenterology. 2016; 30: 145–159. https://doi.org/10.1016/j.bpg.2016.02.007

[71] Ononamadu CJ, Ibrahim A. Molecular docking and prediction of ADME/drug-likeness properties of potentially active antidiabetic compounds isolated from aqueous-methanol extracts of *Gymnema sylvestre* and *Combretum micranthum*. Biotechnologia. 2021; 102: 85–99. https://doi.org/10.5114/bta.2021.103765

[72] Unsal V, Oner E, Yıldız R, Mert BD. Comparison of new secondgeneration H1 receptor blockers with some molecules; a study involving DFT, molecular docking, ADMET, biological target and activity. BMC Chemistry. 2025; 19: 4. https://doi.org/10.1186/s13065-024-01371-4

[73] Kitchen DB, Decornez H, Furr JR, Bajorath J. Docking and scoring in virtual screening for drug discovery: methods and applications. Nature Reviews. Drug Discovery. 2004; 3: 935–949. https://doi.org/10.1038/nrd1549

[74] Khan T, Ali M, Khan A, Nisar P, Jan SA, Afridi S, et al. Anticancer Plants: A Review of the Active Phytochemicals, Applications in Animal Models, and Regulatory Aspects. Biomolecules. 2019; 10: 47. https://doi.org/10.3390/biom10010047

[75] Weyand CM, Goronzy JJ. The immunology of rheumatoid arthritis. Nature Immunology. 2021; 22: 10–18. https://doi.org/10.1038/s41590-020-00816-x

[76] Porchas-Quijada M, Reyes-Castillo Z, Muñoz-Valle JF, Durán-Barragán S, Aguilera-Cervantes V, López-Espinoza A, et al. IgG Anti-ghrelin Immune Complexes Are Increased in Rheumatoid Arthritis Patients Under Biologic Therapy and Are Related to Clinical and Metabolic Markers. Frontiers in Endocrinology. 2019; 10: 252. https://doi.org/10.3389/fendo.2019.00252

[77] Wu Z, Ma D, Yang H, Gao J, Zhang G, Xu K, et al. Fibroblast-like synoviocytes in rheumatoid arthritis: Surface markers and phenotypes. International Immunopharmacology. 2021; 93: 107392. https://doi.org/10.1016/j.intimp.2021.107392

[78] Bustamante MF, Garcia-Carbonell R, Whisenant KD, Guma M. Fibroblast-like synoviocyte metabolism in the pathogenesis of rheumatoid arthritis. Arthritis Research & Therapy. 2017; 19: 110. https://doi.org/10.1186/s13075-017-1303-3

[79] Nygaard G, Firestein GS. Restoring synovial homeostasis in rheumatoid arthritis by targeting fibroblast-like synoviocytes. Nature Reviews. Rheumatology. 2020; 16: 316–333. https://doi.org/10.1038/s41584-020-0413-5

[80] Mateen S, Zafar A, Moin S, Khan AQ, Zubair S. Understanding the role of cytokines in the pathogenesis of rheumatoid arthritis. Clinica Chimica Acta; International Journal of Clinical Chemistry. 2016; 455: 161–171. https://doi.org/10.1016/j.cca.2016.02.010

[81] McInnes IB, Schett G. Cytokines in the pathogenesis of rheumatoid arthritis. Nature Reviews. Immunology. 2007; 7: 429–442. https://doi.org/10.1038/nri2094

[82] Marcucci E, Bartoloni E, Alunno A, Leone MC, Cafaro G, Luccioli F, et al. Extra-articular rheumatoid arthritis. Reumatismo. 2018; 70: 212–224. https://doi.org/10.4081/reumatismo.2018.1106

[83] Ridgley LA, Anderson AE, Pratt AG. What are the dominant cytokines in early rheumatoid arthritis? Current Opinion in Rheumatology. 2018; 30: 207–214. https://doi.org/10.1097/BOR.0000000000000470

[84] Liu J, Tang J, Zuo Y, Yu Y, Luo P, Yao X, et al. Stauntoside B inhibits macrophage activation by inhibiting NF-κB and ERK MAPK signalling. Pharmacological Research. 2016; 111: 303–315. https://doi.org/10.1016/j.phrs.2016.06.022

[85] Schett G, Zwerina J, Firestein G. The p38 mitogen-activated protein kinase (MAPK) pathway in rheumatoid arthritis. Annals of the Rheumatic Diseases. 2008; 67: 909–916. https://doi.org/10.1136/ard.2007.074278

[86] Behl T, Upadhyay T, Singh S, Chigurupati S, Alsubayiel AM, Mani V, et al. Polyphenols Targeting MAPK Mediated Oxidative Stress and Inflammation in Rheumatoid Arthritis. Molecules (Basel, Switzerland). 2021; 26: 6570. https://doi.org/10.3390/molecules26216570

[87] Lee MR, Kim JE, Park JJ, Choi JY, Song BR, Choi YW, et al. Protective role of fermented mulberry leave extract in LPS-induced inflammation and autophagy of RAW264.7 macrophage cells. Molecular Medicine Reports. 2020; 22: 4685–4695. https://doi.org/10.3892/mmr.2020.11563

[88] Yuan W, Song HY, Xiong J, Jiang WL, Kang GJ, Huang J, et al. Placenta-derived mesenchymal stem cells ameliorate lipopolysaccharide-induced inflammation in RAW264.7 cells and acute lung injury in rats. Molecular Medicine Reports. 2020; 22: 1458–1466. https://doi.org/10.3892/mmr.2020.11231

[89] Zhu H, Wang X, Wang X, Liu B, Yuan Y, Zuo X. Curcumin attenuates inflammation and cell apoptosis through regulating NF-κB and JAK2/STAT3 signaling pathway against acute kidney injury. Cell Cycle (Georgetown, Tex.). 2020; 19: 1941–1951. https://doi.org/10.1080/15384101.2020.1784599

[90] Zhang W, Guo H, Li L, Zhang M, Xu E, Dai L. Network Pharmacology-Based Strategy Integrated with Molecular Docking and In Vitro Experimental Validation to Explore the Underlying Mechanism of *Fangji Huangqi* Decoction in Treating Rheumatoid Arthritis. ACS Omega. 2024; 9: 31878–31889. https://doi.org/10.1021/acsomega.4c03495